The Plant Cell, Vol. 26: 3501–3518, September 2014, www.plantcell.org 

# ROP3 GTPase Contributes to Polar Auxin Transport and Auxin Responses and Is Important for Embryogenesis and Seedling Growth in *Arabidopsis*[CW]

**Jia-bao Huang,[a,1] Huili Liu,[a,1] Min Chen,[a,2] Xiaojuan Li,[a] Mingyan Wang,[a] Yali Yang,[a] Chunling Wang,[a] Jiaqing Huang,[a] Guolan Liu,[a] Yuting Liu,[a] Jian Xu,[c] Alice Y. Cheung,[b] and Li-zhen Tao[a,3]**

[a] Guangdong Provincial Key Laboratory of Protein Function and Regulation in Agricultural Organisms, College of Life Sciences, South China Agricultural University, Guangzhou 510642, China

[b] Department of Biochemistry and Molecular Biology, University of Massachusetts, Amherst, Massachusetts 01003

[c] Department of Biological Sciences and NUS Centre for BioImaging Sciences, National University of Singapore, Singapore 117543

**ROP GTPases are crucial for the establishment of cell polarity and for controlling responses to hormones and environmental signals in plants. In this work, we show that ROP3 plays important roles in embryo development and auxin-dependent plant growth. Loss-of-function and dominant-negative (DN) mutations in *ROP3* induced a spectrum of similar defects starting with altered cell division patterning during early embryogenesis to postembryonic auxin-regulated growth and developmental responses. These resulted in distorted embryo development, defective organ formation, retarded root gravitropism, and reduced auxin-dependent hypocotyl elongation. Our results showed that the expression of AUXIN RESPONSE FACTOR5/MONOPTEROS and root master regulators PLETHORA1 (PLT1) and PLT2 was reduced in *DN-rop3* mutant embryos, accounting for some of the observed patterning defects. ROP3 mutations also altered polar localization of auxin efflux proteins (PINs) at the plasma membrane (PM), thus disrupting auxin maxima in the root. Notably, *ROP3* is induced by auxin and prominently detected in root stele cells, an expression pattern similar to those of several stele-enriched *PINs*. Our results demonstrate that ROP3 is important for maintaining the polarity of PIN proteins at the PM, which in turn ensures polar auxin transport and distribution, thereby controlling plant patterning and auxin-regulated responses.**

## INTRODUCTION

Plant Rho-like small G proteins called RAC/ROPs (ROPs will be used from now on) function as molecular switches in diverse signaling cascades and mediate leaf cell morphogenesis, polarized cell growth in pollen tubes and root hairs, and hormone and defense-related responses (Nibau et al., 2006; Yang and Fu, 2007; Yalovsky et al., 2008; Wu et al., 2011). ROPs shuttle between a GTP-bound active form and a GDP-bound inactive form. In their active state, ROPs interact with effector proteins to initiate myriad downstream signaling pathways.

The *Arabidopsis thaliana* genome encodes 11 ROPs. We have previously demonstrated that several members of the *Arabidopsis* ROP family and RAC1 from tobacco (*Nicotiana tabacum*) mediate auxin-signaled gene expression and that perturbing the signaling capacity of these small GTPases induces auxin-related developmental defects (Tao et al., 2002, 2005). The precise contribution from individual ROPs to auxin signaling remains largely unknown. Recent studies have indicated the involvement of ROP signaling in the regulation of polar auxin transport, which generates auxin gradients and underlies almost all aspects of auxin controlled growth and developmental responses. ROP2 has been implicated in the regulation of PIN1 endocytosis in the leaf epidermal pavement cells (Nagawa et al., 2012). ROP6, together with its effector RIC1 (ROP-interactive CRIB motif-containing protein1), control clathrin-dependent PIN1/PIN2 endocytosis and mediate root gravitropic responses and leaf vasculature development (Chen et al., 2012; Lin et al., 2012). A ROP effector protein ICR1 (interactor of constitutive active ROP1) is required for embryo development, root meristem organization, and polar localization of PIN1 and PIN2 (Hazak et al., 2010).

Polar auxin transport is mediated by the PIN family of auxin efflux proteins and the AUX1/LAX family of influx carrier proteins (Bennett et al., 1996; Swarup et al., 2008). Genetic elimination of components in auxin transport, e.g., by mutations in members of the PIN proteins, such as *PIN1*, *3*, *4*, and *7* (Friml et al., 2003; Blilou et al., 2005), underlies defects in many auxin-regulated processes. Of the PINs, PIN1 is involved in the mediation of auxin accumulation in the base of early globular embryos to initiate hypophysis specification and postembryonic root growth (Petricka et al., 2012). PIN3 is required for auxin flow to the root tip and redistribution within root tissues, which influences tropic responses (Friml et al., 2002; Blilou et al., 2005; Grieneisen et al., 2007). PIN proteins exhibit polar localization at the plasma membrane and determine the direction of intercellular auxin flow

[1] These authors contributed equally to this work.

[2] Current address: College of Life and Environmental Sciences, University of Exeter, Exeter EX44QD, UK.

[3] Address correspondence to lztao2005@scau.edu.cn.

The author responsible for distribution of materials integral to the findings presented in this article in accordance with the policy described in the Instructions for Authors (www.plantcell.org) is: Li-zhen Tao (lztao2005@scau.edu.cn).

[C] Some figures in this article are displayed in color online but in black and white in the print edition.

[W] Online version contains Web-only data.

www.plantcell.org/cgi/doi/10.1105/tpc.114.127902

(Wisniewska et al., 2006). PIN polar localization and asymmetric auxin distribution are regulated by multiple factors, including regulated endocytosis, recycling, and retromer-dependent vacuolar targeting (Steinmann et al., 1999; Geldner et al., 2003; Jaillais et al., 2007; Kleine-Vehn et al., 2008b). In addition, phosphorylation and dephosphorylation cycles mediated by the AGC kinases PINOID (PID) and PID-related AGC3 and the phosphatase PP2A are important for dynamic changes of PIN polarity. Both PID and PP2A have been shown to be required for auxin transport-related embryo development and postembryonic organogenesis (Christensen et al., 2000; Friml et al., 2004; Michniewicz et al., 2007; Dhonukshe et al., 2010).

How ROPs regulate auxin-dependent development remains largely unknown. RopGEFs are guanine nucleotide exchange factors (GEFs) that stimulate GDP-GTP exchange and activate ROPs (Berken et al., 2005). We showed recently that one of the 14 *Arabidopsis* ROPGEFs, RopGEF7, is important for embryo and root meristem pattern formation controlled by the auxin/PLETHORA (PLT)-dependent pathway (Chen et al., 2011). We also established that ROP3 interacts directly with RopGEF7 (Chen et al., 2011). Here, we explore the developmental role of ROP3 by analyzing *rop3* T-DNA insertion and dominant-negative *rop3* mutant lines. Mutant phenotypes show that ROP3 has broad biological roles and is important for the regulation of embryo development, postembryonic organ formation, root gravitropism, hypocotyl elongation, and root growth sensitivity to auxin. During embryogenesis, perturbing ROP3 function reduces PIN1 abundance in the plasma membrane (PM), whereas in the seedling stage, it causes a basal to apical shift of PIN1 and PIN3 localization. Our data indicate that ROP3 acts in polar auxin transport and thus controls the establishment of auxin maxima, which underlies embryo development and seedling growth.

## RESULTS

### *ROP3* Is Expressed in Developing Embryos and Postembryonic Stages

We used a *ROP3*$_{pro}$*:GUS* (β-glucuronidase) gene fusion to study the spatial expression pattern of *ROP3*. Analysis of GUS activity in *ROP3*$_{pro}$*:GUS* lines revealed that *ROP3* was expressed in embryonic and postembryonic stages (Figure 1; Supplemental Figure 1). In globular stage embryos, GUS activity was detected only in the hypophysis (Figure 1C). At the heart and late heart stages, GUS activity was maintained in the daughter cells of the hypophysis (Figures 1D and 1E). During the late stages, GUS activity was also detected in the tip regions of cotyledons in addition to the root pole (Figure 1F). When GUS staining duration was prolonged from 16 to 36 h, GUS activity could be detected in the embryo proper, but not in the hypophysis at the octant (Figure 1A) and 16-cell stages (Figure 1B), indicating that ROP3 is expressed in the earliest stage of embryo development. In the seedling stage, we found GUS signals in the root, hypocotyl, and cotyledons (Figure 1G). Upon closer examination of root tips, the region that showed the GUS staining appeared to be in the quiescent center, columella stem cells, and columella cell layers (Figure 1J, left), and stele cells in root meristem showed relatively weak GUS signal (Figure 1H). *ROP3* was also expressed in guard cells of cotyledons (Supplemental Figure 1A) and at a much higher level in the anther and pollen (Supplemental Figures 1B and 1C). The observed *ROP3*$_{pro}$*:GUS* expression profile matches the results of public expression databases (e.g., http://www.ebi.ac.uk/arrayexpress). For instance, the pattern in seedling roots as visualized by GUS reporter gene expression was consistent with microarray results for *ROP3* from different root sections (Dinneny et al., 2008; http://bar.utoronto.ca/efp/cgi-bin/efpWeb.cgi?dataSource=Root). To further validate this observation, we performed quantitative RT-PCR (qRT-PCR) analysis on root sections. The results showed that *ROP3* was expressed in root columella and meristem, elongation, and maturation regions (Supplemental Figure 1D). The expression level of *ROP3* was relatively higher in the root columella and meristem and elongation zones in contrast to that in the root maturation zone (Supplemental Figure 1D). This result is consistent with data from microarray analysis of root sections (Dinneny et al., 2008).

We also examined whether *ROP3* expression is influenced by auxin. qRT-PCR analysis showed that the expression of *ROP3* was induced by auxin in the roots of seedlings. Treatment with 10 μM 1-naphthaleneacetic acid (NAA) for 12 h clearly enhanced the transcript levels of *ROP3*, reaching the highest level after 24 h of NAA treatment (Figure 1I). Further study using transgenic plants expressing *ROP3*$_{pro}$*:GUS* confirmed that auxin treatment increased the expression of *ROP3*, which is detectable at the elongation zone of the primary roots (Figure 1J), consistent with *ROP3* being involved in auxin-regulated pathways.

We next constructed a fusion to yellow fluorescent protein (YFP) to examine the subcellular localization of ROP3 in root cells (Supplemental Figures 1E to 1H). YFP:ROP3 was predominantly localized in the PM of root cells (Supplemental Figures 1E and 1F). We also examined the subcellular localization of the dominant negative DN-rop3 (see below) and found that in roots, YFP:DN-rop3 showed diminished PM accumulation and was mainly detected in the cytoplasm and the perinuclear region (Supplemental Figures 1G and 1H).

### Ectopic Expression of *DN-rop3* or Loss of Function in *ROP3* Affects Embryo Patterning

Replacement of specific amino acid residues in GTP binding domain in ROPs is a commonly used and informative method to create dominant mutations in these small GTPases (Feig, 1999; Yang, 2002). Based on this, we constructed the dominant-negative (DN) mutant *DN-rop3*, which presumably locks ROP3 in the inactive form, and explored the functional role of *ROP3* in embryo development in *DN-rop3* transgenic plants. A majority of plants transformed with *DN-rop3* under a strong embryonic promoter *RPS5A* (Weijers et al., 2001) (81% of individual lines [38/47]) displayed embryo phenotype. Analysis of transcription in these *DN-rop3* lines by qRT-PCR and immunoblot detection by ROP3 antibody showed that their embryo defects increased with increasing expression of the *DN-rop3* transgene (Supplemental Figures 2A to 2D).

In the embryos, overexpression of *DN-rop3* produced a range of cell division defects from one-cell to heart embryo stages (Supplemental Table 2). The wild-type zygote elongates after fertilization and undergoes an asymmetric cell division to result in a small apical cell and a large basal cell (Figure 2A). In contrast

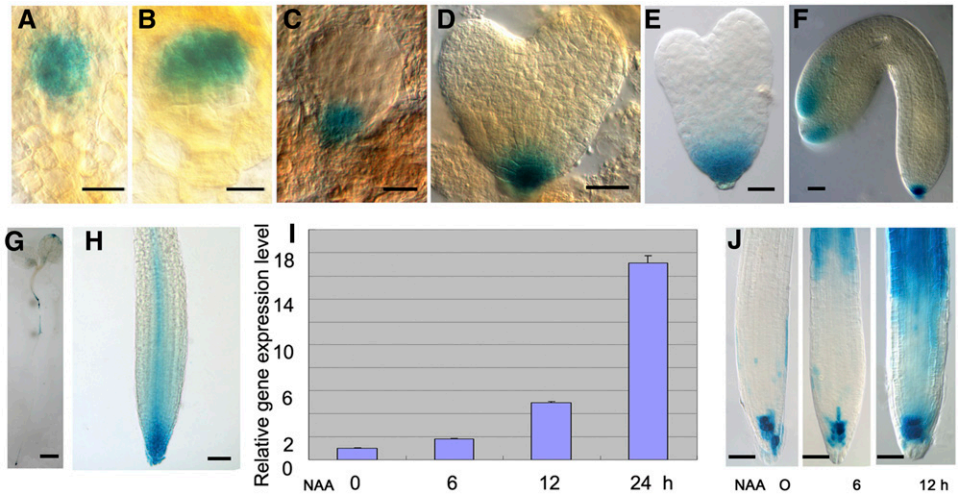


**Figure 1.** Expression of *ROP3*$_{pro}$*:GUS*.

**(A)** to **(F)** *ROP3*$_{pro}$*:GUS* is expressed in octant **(A)**, 16-cell **(B)**, globular **(C)**, heart **(D)**, late heart **(E)**, and bent **(F)** embryo stages.
**(G)** and **(H)** *ROP3*$_{pro}$*:GUS* is expressed in a 5-d-old seedling **(G)** and root tip **(H)**.
**(I)** qRT-PCR analysis showed that *ROP3* expression in roots of 7-d-old wild-type seedlings was enhanced by 10 μM NAA treatment for various times, as indicated.
**(J)** GUS staining showed that GUS activity in roots of 5-d-old *ROP3*$_{pro}$*:GUS* seedlings is induced by 10 μM NAA for 6 (middle) and 12 (right) h; untreated sample is used as control (left).
GUS staining was for 36 h in **(A)** and **(B)**, 16 h in **(C)** to **(H)**, and 6 h in **(J)**. Bars = 10 μm in **(A)** to **(C)**, 20 μm in **(D)** to **(F)**, 1mm in **(G)**, and 50 μm in **(H)** and **(J)**.

to the asymmetric cell division in the wild-type embryos, *DN-rop3* zygotes divided more symmetrically, giving rise to almost equal-sized apical and basal cells (Figure 2E). At the two-cell to octant embryo stages, abnormal transverse cell divisions were observed in the apical cell, forming a file of cells (Figures 2F and 2G), while the apical cell in the wild-type embryo divides vertically (Figure 2B) with the basal cell dividing anticlinally to form the suspensor (Figure 2B). At the four-cell stage, suspensor cells displayed aberrant periclinal cell divisions in *DN-rop3* embryos (Figures 2H and 2I compared with 2C). When *DN-rop3* embryos reached the eight-cell stage, both the apical domain and the suspensor showed cell division defects (Figures 2J and 2K compared with 2D). At 16- and 32-cell stages, tangential divisions separate the protoderm from the inner cells in wild-type embryos (Figures 3A and 3B), whereas *DN-rop3* embryos displayed abnormal cell divisions at the apical domain (Figures 3F and 3G). In addition to the phenotypes in the embryo proper, periclinal divisions in the hypophyseal cell and adjacent suspensor cell occurred in *DN-rop3* embryos, while no cell division occurred in the hypophysis and normal anticlinal divisions occurred in wild-type suspensors (Figures 3F and 3G compared with 3A and 3B). From the globular to the heart embryo stage, cell division defects in the hypophysis were frequently observed in *DN-rop3* embryos, resulting in aberrant organization of the root stem cell niche (Figures 3H to 3J compared with 3C to 3E). Together, the defects in *DN-rop3* are consistent with ROP3 being important in promoting the normal pattern formation during embryo development.

To ascertain the role of *ROP3* in embryo development, we obtained lines with T-DNA insertions in the fifth and third exon (SALK_008896 and SALK_0325580C, respectively) of *ROP3*. These mutants are designated *rop3-1* and *rop3-2*, respectively (Supplemental Figure 3A). qRT-PCR analysis showed absence of *ROP3* transcripts in these T-DNA insertion lines, confirming that they are null mutants (Supplemental Figure 3B). Disruption of *ROP3* causes defects in asymmetric division of the zygotes (Figures 2L and 2M) and cell division orientation in the apical (Figure 2N) and suspensor cells (Figures 2O to 2Q) during early stages of embryogenesis. *rop3* embryos have enlarged suspensors with periclinal cell divisions (Figures 3K and 3M) and abnormal cell divisions in the hypophysis, leading to aberrations in the basal embryo region (Figure 3K to 3O). The embryo phenotype in *rop3* knockout mutants was indistinguishable from the phenotype of *DN-rop3* embryos, although the severity differed between these mutants. For instance, a higher percentage of zygotes divided symmetrically in *rop3* mutants than in *DN-rop3* (*rop3-1*, 16.0%, $n$ = 50; *rop3-2*, 13.0%, $n$ = 46 versus *DN-rop3* L12, 11.7%, $n$ = 60; L16, 12.5%, $n$ = 40; Supplemental Table 2). When these mutant embryos reached later development stages, the percentage of cell division defects in *rop3* become lower than *DN-rop3* (*rop3-1*, 8.1%, $n$ = 867; *rop3-2*, 7.96%, $n$ = 1043 versus *DN-rop3* L16, 23.3%, $n$ = 748; L12, 16.01%, $n$ = 537; Supplemental Table 2). The overall lower frequency of cell division defects (Supplemental Table 2) in developing *rop3* embryos suggests that other *ROPs* might be expressed after the zygotic division stage, compensating for the requirement for ROP3.

To verify whether the *rop3* embryo phenotype is caused by *rop3* deficiency, transgenic plants containing the coding region of *ROP3* driven by its endogenous *ROP3* promoter (*ROP3*$_{pro}$*:ROP3*) were crossed with *rop3-1* and *rop3-2* mutants. Homozygous lines were obtained and used for subsequent analysis.

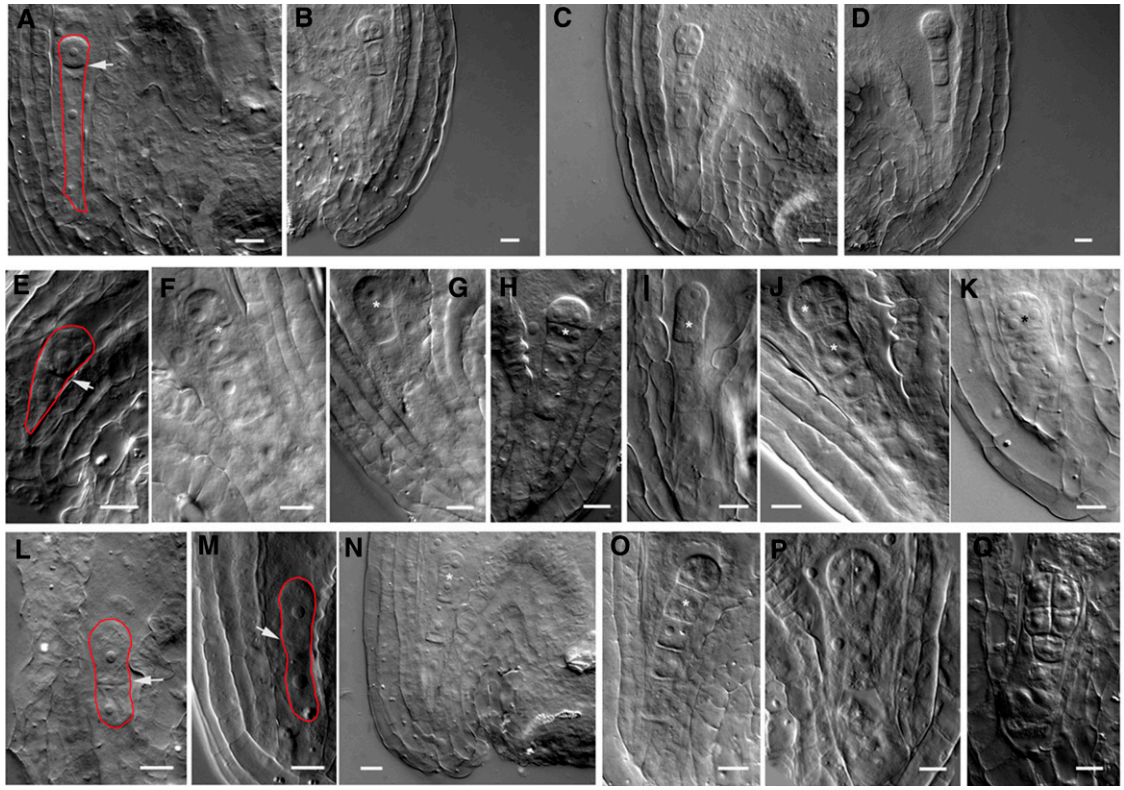


**Figure 2.** *DN-rop3* and *rop3* Mutants Display Aberrant Division Patterns in Early Embryogenesis.

**(A)** to **(D)** Wild-type embryos at zygotic division **(A)**, two-cell **(B)**, four-cell **(C)**, and eight-cell **(D)** stages.
**(E)** to **(K)** Embryos from *RPS5A*$_{pro}$*:DN-rop3* transgenic plants at zygotic division **(E)**, two-cell (**[F]** and **[G]**), four-cell (**[H]** and **[I]**), and eight-cell (**[J]** and **[K]**) stages.
**(L)** to **(Q)** *rop3* embryos at zygotic division (**[L]** and **[M]**), two-cell **(N)**, four-cell (**[O]** and **[P]**), and eight-cell **(Q)** stages.
Arrows mark the cell plates between the apical and basal daughter cells of the zygote. Asterisks denote aberrant cell divisions. Red lines outline the zygotes. Bars = 10 μm.

The recovered expression levels of *ROP3* in *rop3-1* and *rop3-2* lines were confirmed by qRT-PCR (Supplemental Figure 4A). The *ROP3*$_{pro}$*:ROP3* transgene can fully rescue the phenotypes of *rop3* mutants, including their embryo phenotype (Supplemental Figures 4F to 4K compared with 4C to 4E and Supplemental Table 4 online).

## ROP3 Regulates Auxin-Related Postembryonic Development

To further investigate the requirement of *ROP3* for plant development, we analyzed the seedling phenotype of plants transformed by 35S promoter-driven *DN-rop3* (*35S*$_{pro}$*:DN-rop3*) and *rop3* mutants. Twenty-five individual *35S*$_{pro}$*:DN-rop3* transgenic plants were generated; these plants showed different levels of transgene expression (Supplemental Figures 2B and 2D). Two homozygous lines (L2 and L3), containing a T-DNA insertion at a single locus, were chosen for subsequent analysis. In contrast to the wild type (Figure 4B), progeny from L2 and L3 displayed a variety of developmental aberrations, ranging from altered cotyledon numbers (Figures 4F to 4H) to lack of roots (Figures 4D and 4E) or of both hypocotyls and roots (Figure 4C). Lugol staining of starch granules as a marker for columella cell differentiation revealed a loss of columella stem cells and disorganization of columella cells (Figures 4T to 4V compared with 4S). The most commonly observed seedling phenotype was the development of short roots (Figure 4A, right; Supplemental Table 3), consistent with their having resulted from the disruption of proper patterning in the root stem cell niche (Figures 4T to 4V, compared with 4S). Occasionally, the strong *DN-rop3* lines produce offspring with two shoots sharing one primary root (Figure 4I). In some cases, *DN-rop3* seedlings have one shoot with two roots fused to each other (Figure 4J). In addition to these root phenotypes, a low percentage of *35S* $_{pro}$*:DN-rop3* seedlings (L2, 5.6%, $n$ = 215; L3, 3.4%, $n$ = 232; wild type, 0%, $n$ = 327; Supplemental Table 3) showed severe defects in cotyledon development, including no or single cotyledons, and completely fused cotyledons (Figures 4F to 4H), phenotypes that were also observed in transgenic tobacco with *RAC1* downregulated by RNA interference (RNAi) (Tao et al., 2002). The pronounced patterning defects in *DN-rop3* seedlings also resemble those of auxin mutants defective in auxin transport and signaling such as *pin* multiple mutants, *gnom*, *bodenlos*, and *monopteros* (*mp*) (Friml et al., 2003; Lau et al., 2012).

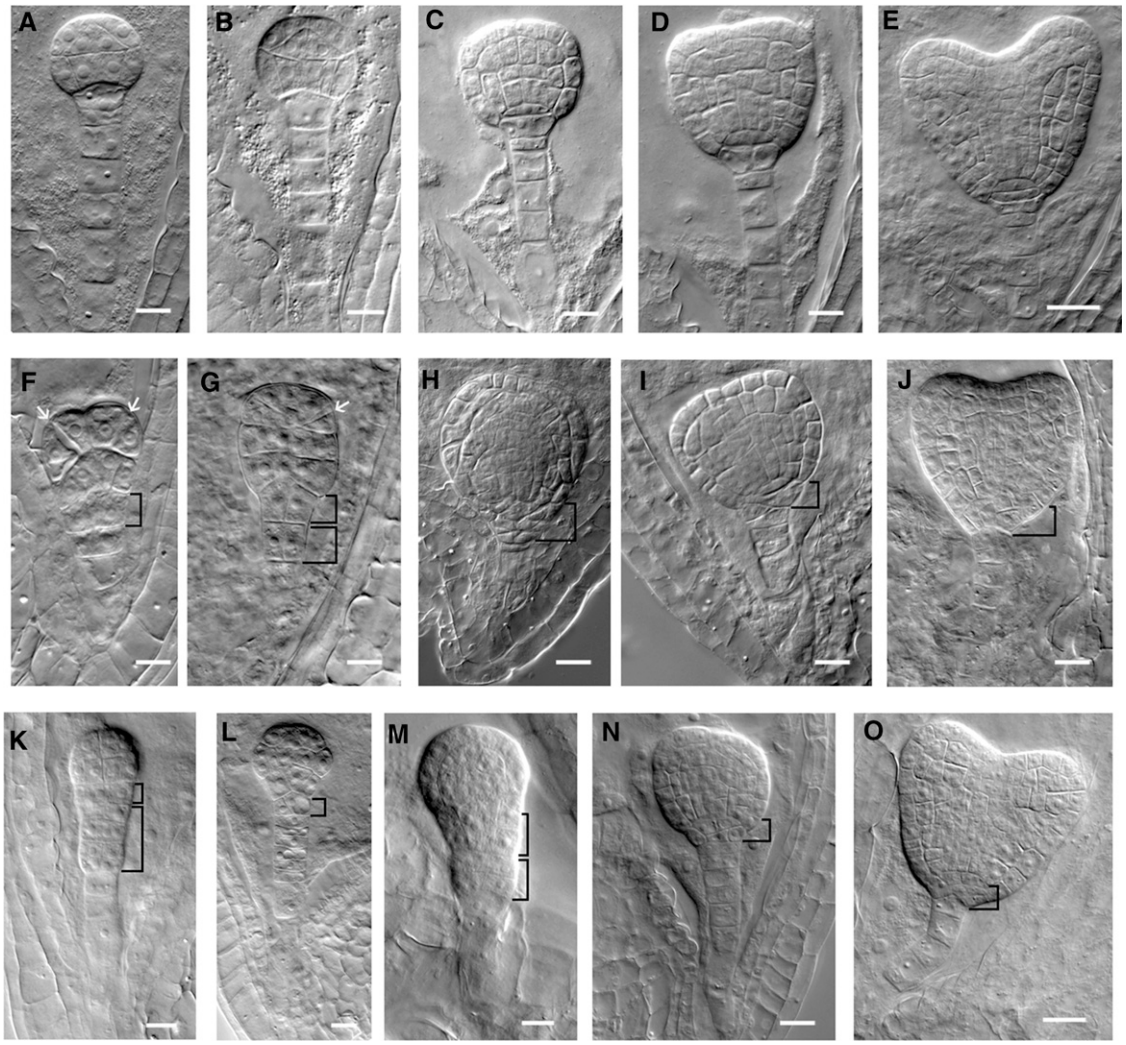


**Figure 3.** *DN-rop3* and *rop3* Mutants Have Defective Cell Divisions in the Basal Lineage of the Embryos.

**(A)** to **(E)** Wild-type embryos at 16-cell **(A)**, 32-cell **(B)**, globular **(C)**, triangle **(D)**, and heart **(E)** stages.
**(F)** to **(J)** Embryos of *RPS5A*$_{pro}$*:DN-rop3* transgenic plants at 16-cell **(F)**, 32-cell **(G)**, globular **(H)**, triangle **(I)**, and heart **(J)** stages. Arrows indicate the position of aberrant cell division plate.
**(K)** to **(O)** *rop3* embryos at 16-cell **(K)**, 32-cell **(L)**, globular **(M)**, triangle **(N)**, and heart **(O)** stages. Bracketed area displays cell division defects in basal embryo region, and the lower one in **(G)**, **(K)**, and **(M)** shows abnormal cell divisions in suspensor cells.
Bars = 20 μm in **(E)**, **(J)**, and **(O)** and 10 μm for the rest of the images.

We also analyzed the seedling phenotype of *rop3* mutants. Both *rop3-1* (Figure 4K) and *rop3-2* (Figure 4L) displayed defects in root growth (Figures 4N to 4P compared with 4M; Supplemental Table 3) and cotyledon development (Figures 4Q and 4R) similar to phenotypes of *DN-rop3* transgenic plants. The frequency of defective *rop3* seedlings was nevertheless lower than that observed in the progeny of *DN-rop3* lines (*DN-rop3-L2*, 36.3%, $n$ = 215; L3, 41.31%, $n$ = 232; *rop3-1*, 15.8%, $n$ = 298; *rop3-2*, 10.64%, $n$ = 356; Supplemental Table 3).

Under normal growth conditions, the progeny of *DN-rop3* and *rop3* mutants segregated a variety of phenotypes. For instance, some *rop3* seedlings displayed severe defects in organ formation, including cotyledons and roots (Figure 4), while some appeared to be normal. We therefore decided to test whether the *35S*$_{pro}$*:DN-rop3* and *rop3* seedlings, including normal-looking ones, showed altered growth responses to gravity and exogenous auxin. We first examined the root gravitropic responses in *DN-rop3* and *rop3* mutants. Unlike the wild type, the roots of *DN-rop3* and *rop3* were less sensitive to gravity, based on measurement of root curvature after gravity stimulation (Figure 5A). We next tested whether the sensitivity to applied auxin was also affected in *DN-rop3* and *rop3*. Exogenous auxin inhibited root elongation of wild-type seedlings, but *DN-rop3* and *rop3* roots were more resistant to auxin inhibition over a range of hormone concentrations (Figure 5B). The difference from the wild type was especially notable at low auxin concentrations, e.g., 50 nM NAA, where the root

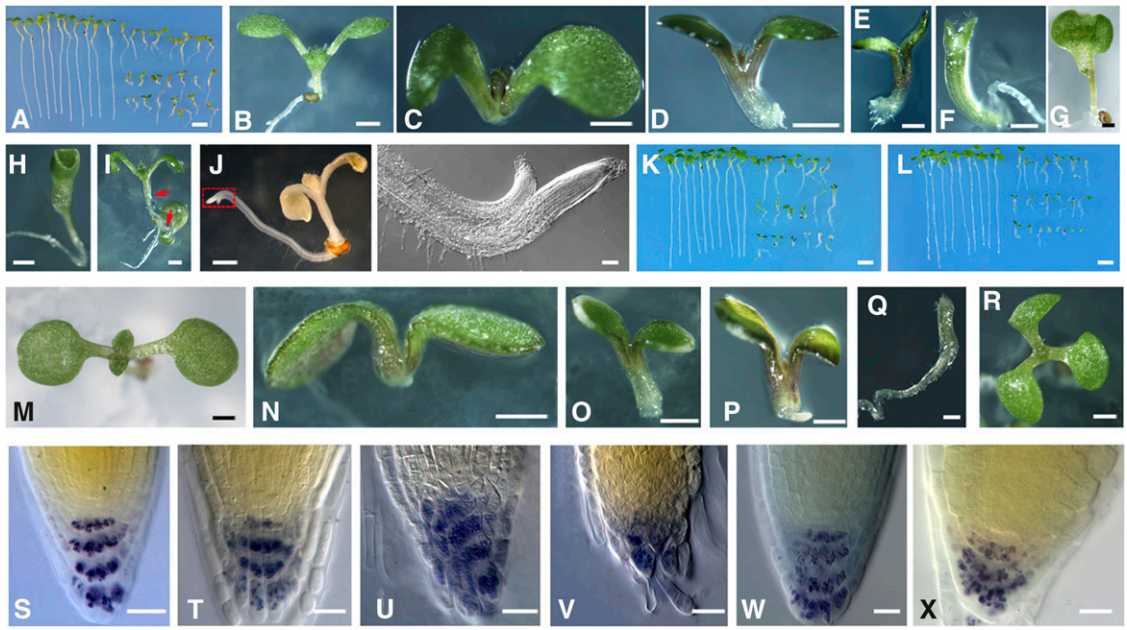


**Figure 4.** *DN-rop3* and *rop3* Seedling Phenotypes.

**(A)** Comparison of 7-d-old seedlings between the wild type (left) and progenies of *DN-rop3* transgenic plants (right).
**(B)** Seven-day-old wild-type seedlings.
**(C)** to **(I)** Phenotypes of 7-d-old progeny seedlings of *DN-rop3* transgenic plants. Red arrows in **(I)** point to the shoots.
**(J)** Seven-day-old seedling of *DN-rop3* (left), boxed area was magnified (right).
**(K)** Comparison of 7-d-old seedlings between the wild type (left) and *rop3-1* (right).
**(L)** Comparison of 7-d-old seedlings between the wild type (left) and *rop3-2* (right).
**(M)** Seven-day-old wild-type seedlings.
**(N)** to **(R)** *rop3* seedlings.
**(S)** to **(X)** Lugol-stained root tip of 7-d-old wild type (**[S]** and **[W]**), *DN- rop3* (**[U]** to **[V]**), and *rop3* **(X)** seedlings.
Bars = 1 mm in **(B)** to **(J)** and **(M)** to **(R)**, 5 mm in **(A)**, **(K)**, and **(L)**, 20 μm in **(S)** to **(X)**.

length of *DN-rop3* and *rop3* was almost not affected compared with 15% growth inhibition shown by wild-type seedlings (Figure 5B). At 100 nM NAA, wild-type root length was reduced to 69% of that of untreated seedlings, whereas *DN-rop3* and *rop3* roots displayed considerably less inhibition, with root length being around 90% and over 80%, respectively, of that of the corresponding untreated seedlings (Figure 5B), indicating that *DN-rop3* and *rop3* mutants have impaired auxin responses.

We also analyzed the effect of hypocotyl elongation under high temperature (29°C), another well-established auxin-dependent process because high temperature has been shown to induce higher level of auxin and therefore stimulates hypocotyl elongation (Gray et al., 1998). Seedlings of *DN-rop3* and *rop3* mutants were clearly less responsive to high temperature in stimulated hypocotyl elongation than the wild type (Figure 5C), suggesting repressed auxin responses in *DN-rop3* and *rop3* mutants.

As *ROP3* is expressed in pollen (Supplemental Figure 1C) and therefore likely plays a role in pollen development similar to the closely related genes *ROP1* and *ROP5* (Craddock et al., 2012). Our analysis of *rop3* mutants did not show any notable pollen development phenotype, germination in vivo, and tube growth properties in the pistil (Supplemental Figure 5). However, we could not rule out the possibility that *ROP3* functions in pollen, since two other pollen-expressed ROPs, *ROP1* and *ROP5*, are abundantly expressed there. In fact, *ROP1* and *ROP5* had been shown to play roles in pollen tube polar growth by gain-of-function studies (Kost et al., 1999; Li et al., 1999; Gu et al., 2003)

## ROP3 Regulates the Establishment of Auxin Maxima in the Embryos and Roots

Phenotypic analyses (Figures 2 to 5) suggest that auxin distribution and responses are affected in *DN- rop3* and *rop3* mutants. To explore this, we analyzed the expression of the auxin reporter *DR5rev:GFP* (for green fluorescent protein; Benková et al., 2003) in the *DN-rop3* and *rop3* backgrounds. As expected, an auxin maximum was detected at the root pole of wild-type embryos (100%, $n$ = 53; Figure 6A). In contrast, this auxin maximum was strongly reduced in a large majority of *DN-rop3* embryos (63/66; Figure 6B), although in a small number (3/66) of embryos, the *DR5rev:GFP* signal was spread out everywhere (Figure 6C). In *rop3* embryos, we also observed reduced DR5 activity at the root pole (49/52; Figure 6E) and altered pattern of DR5 activity in a small number (3/52) of the analyzed embryos (Figure 6F).

We next examined DR5 activity in *DN-rop3* and *rop3* mutant roots. In comparison to wild type, the DR5 activity was highly

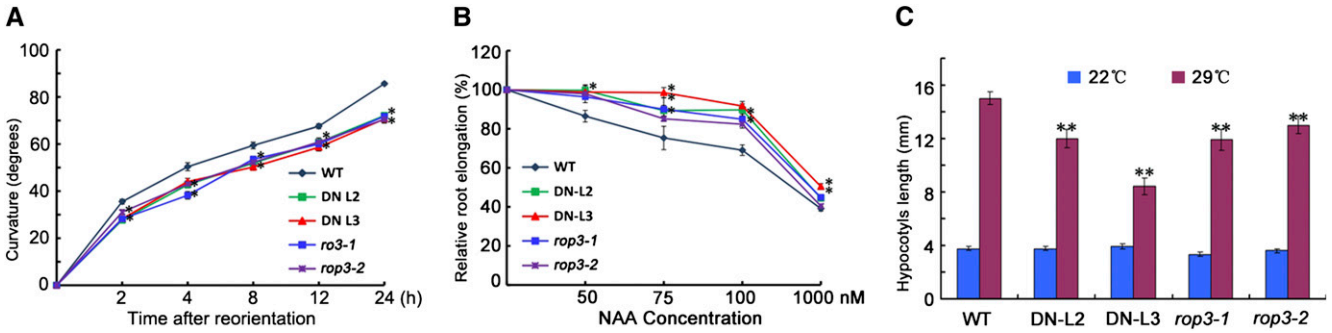


**Figure 5.** *DN-rop3* and *rop3* Mutants Display Reduced Responses to Auxin.

**(A)** Time course of curvature in root gravitropic response tests. Root gravitropic responses of *35S$_{pro}$:DN-rop3* transgenic lines (L2 and L3) and *rop3* knockout mutants (*rop3-1* and *rop3-2*) are compared with the wild-type controls. Curvatures were measured at different time as indicated after reorientation. Data are means ± SD ($n$ = 30 to 50). Asterisks indicate significant differences from the wild type by Student's $t$ test (*P < 0.05; **P < 0.01).
**(B)** Measurement of relative root elongation of seedlings grown on medium supplemented with different concentrations of NAA compared the sensitivity to auxin of *35S$_{pro}$:DN-rop3* transgenic lines (L2 and L3), *rop3* knockout mutants (*rop3-1* and *rop3-2*), and wild-type control. Primary root lengths of untreated plants were set as 100%. Data are means ± SD ($n$ = 30 to 50). Asterisks indicate significant differences from the wild type by Student 's $t$ test (*P < 0.05; **P < 0.01).
**(C)** Hypocotyl lengths of 7-d-old seedlings grown at 22 and 29°C were measured for *35S$_{pro}$:DN-rop3* transgenic lines (L2 and L3), *rop3* knockout mutants (*rop3-1* and *rop3-2*), and wild-type control. Data are means ± SD ($n$ = 30 to 50). Asterisks indicate significant differences from the wild type by Student's $t$ test (*P < 0.05; **P < 0.01).

suppressed in *DN-rop3* (Figure 6H compared with 6G) and was clearly albeit less drastically reduced in *rop3* roots (Figure 6J compared with 6I). These observations suggested that the establishment of auxin maxima was disturbed in *DN-rop3* and *rop3* embryos and roots, correlating with aberrant cell divisions observed in the basal region of their embryos and root tips.

### ROP3 Regulates the Expression of *MP* and PLT1/ PLT2

The phenotypes of *DN-rop3* and *rop3* mutants, together with *DR5rev:GFP* expression defects, suggest that *ROP3* participates in auxin-mediated embryo patterning and root growth. To further address this issue, we focused on whether *ROP3* affects some of the regulators that control cell fate specification events in embryogenesis and root meristem establishment, including *MP*, encoding auxin response factor 5, and root stem cell determinants PLT1 and PLT2, whose expression is dependent on auxin (Aida et al., 2004; Galinha et al., 2007). We first analyzed *MP* expression, as revealed by the marker *MP$_{pro}$:n3XGFP* (Rademacher et al., 2012), in *DN-rop3* and *rop3* mutant embryos. The expression of *MP* was drastically altered in both *DN-rop3* (Figures 7B and 7D compared with 7A and 7C) and *rop3* embryos (Figures 7F and 7H compared with 7E and 7G). Next, we investigated whether ROP3 was involved in the regulation of PLTs and examined the expression of *PLT1* and *PLT2* in *DN-rop3* and *rop3* embryos. The expression of PLT1$_{pro}$:PLT:YFP and PLT2 $_{pro}$:PLT2:YFP was significantly reduced in *DN-rop3* and *rop3* embryos from the levels seen in the wild type (Figures 8A to 8F and 8M); these data indicate that ROP3 is important for maintaining MP and PLT1/PLT2 expression and imply a role for this GTPase in the regulation of cell fate identity and embryo polar axis formation.

Downregulation of PLT1:YFP was observed in 62.5% of *DN-rop3* ($n$ = 40) and 27.8% of *rop3* roots ($n$ = 36) compared with the wild type (0%, $n$ = 30) (Figures 8G to 8I). Similarly, the expression of PLT2: YFP was altered in 40.0% of *DN-rop3* ($n$ = 30) and 20.8% of *rop3* ($n$ = 48) in contrast to the wild type (0%, $n$ = 30) (Figures 8J to 8L), indicating that the observed seedling root meristem defects in *rop3* mutants had resulted from the altered PLT1 and PLT2 expression.

### ROP3 Regulates the Polar Localization and Expression of PIN1 and PIN3

We next determined whether the altered DR5 activity during embryogenesis and root growth in *DN-rop3* and *rop3* mutants associate with alterations in auxin transport. The expression and localization of PIN1$_{pro}$:PIN1:GFP was examined in *DN-rop3* and *rop3* embryos. Wild-type embryos showed the normal accumulation of PIN1:GFP (Figure 9A), while a severe reduction of PIN1:GFP in the PM was observed in the cotyledons and provascular cells of the central axis in *DN-rop3* and *rop3* mutant embryos (Figures 9B and 9C). Reduced presence of PIN1:GFP from the PM apparently led to the loss of polarity of PIN1:GFP distribution in the affected cells (Figures 9B and 9C). Moreover, PIN1:GFP labeling was found within intracellular aggregates in the embryo cells in *DN-rop3* and *rop3* mutants (Figures 9B and 9C), indicating that ROP3 is required for the localization of PIN1 to the PM, thereby affecting polar auxin transport during embryo development.

We also analyzed the localization and expression of PIN1:GFP, PIN2:GFP, and PIN3:GFP in the roots of *DN-rop3* and *rop3* mutants. In wild-type roots, PIN1:GFP was localized in the basal membrane of the stele cells (100%, $n$ = 34; Figures 9D and 9E). However, the polarity of PIN1:GFP was changed in the root stele cells of *DN-rop3* (41.3%, $n$ = 80) and *rop3* (20%, $n$ = 60) mutants, where PIN1:GFP was mainly detected in the apical PM instead of the basal side of the stele cells (Figures 9F to 9I). In addition, there were ~30% ($n$ = 80) of *DN-rop3* and 15% ($n$ = 60) of *rop3* mutant roots, which displayed reduced PIN1:GFP

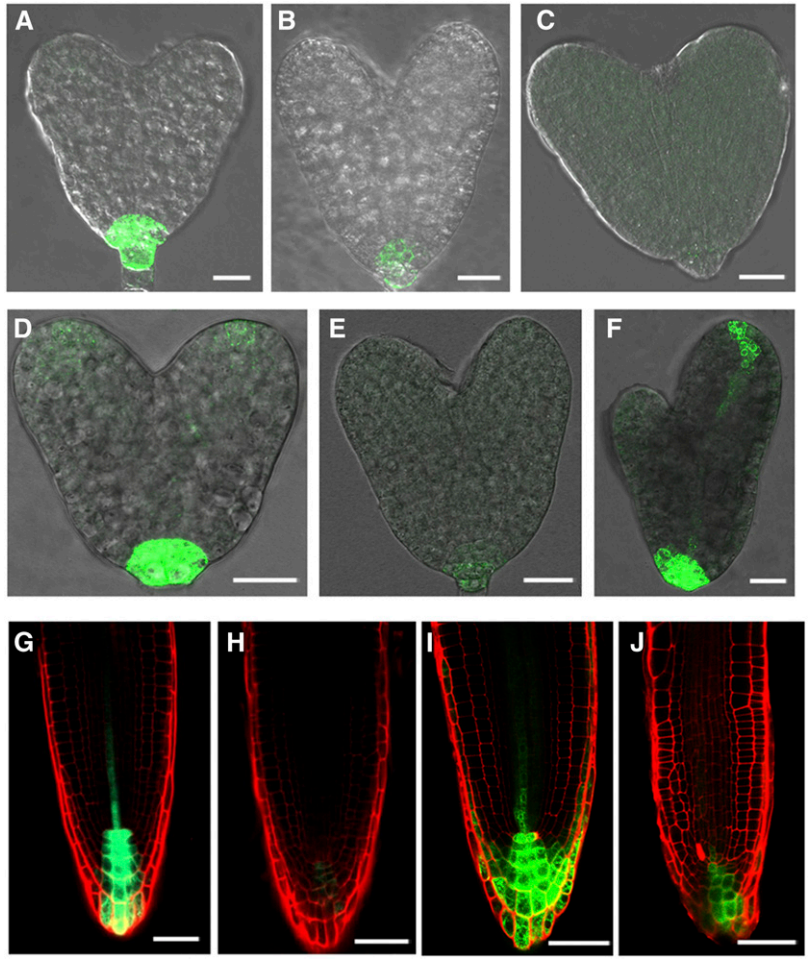


**Figure 6.** *ROP3* Regulates the Maintenance of the Auxin Maximum.

**(A)** to **(C)** *DR5rev:GFP* expression in heart embryos of the wild type **(A)** and *RPS5A*$_{pro}$*:DN-rop3* (**[B]** and **[C]**).
**(D)** to **(F)** *DR5rev:GFP* expression in embryos of the wild type **(D)** and *rop3* (**[E]** and **[F]**).
**(G)** to **(J)** *DR5rev:GFP* expression in roots of 4-d-old wild-type (**[G]** and **[I]**), *35S*$_{pro}$*:DN-rop3* **(H)**, and *rop3* **(J)** seedlings.
Bars = 20 μm in **(A)** to **(F)** and 50 μm in **(G)** to **(J)**.

accumulation (Supplemental Figures 6A to 6C). Similarly, we analyzed the expression and localization of PIN3:GFP in the roots of the *DN-rop3* and *rop3* mutants. Unlike in wild-type roots, which all showed normal accumulation of PIN3$_{pro}$:PIN3:GFP (100%, $n$ = 37; Figures 9J and 9K), *DN-rop3* (28%, $n$ = 50) and *rop3* roots (24%, $n$ = 32) showed a basal to apical shift of PIN3 localization in root stele cells (Figures 9L to 9O). *DN-rop3* (24%, $n$ = 50) and *rop3* roots (22%, $n$ = 32) also showed reduced abundance of PIN3:GFP in the stele and root columella cells (Supplemental Figures 6E and 6F) relative to the wild type (Supplemental Figure 6D). Our previous work on the ROP activator RopGEF7 showed that downregulation of *RopGEF7* by the RNAi technique resulted in reduced accumulation of PIN1$_{pro}$:PIN1:GFP in embryos and roots (Chen et al., 2011). Here, we also examined the polarity of PIN1 and PIN3 in these *RopGEF7RNAi* roots. However, the polarity of PIN1$_{pro}$:PIN1:GFP in *RopGEF7RNAi* roots was not obviously different from that in the wild type (Supplemental Figures 9A and 9B). Similarly, we observed reduced PIN3$_{pro}$:PIN3:GFP accumulation, but no obvious polarity change in *RopGEFRNAi* roots compared with the wild type (Supplemental Figures 9C and 9D).

To determine whether the reduced PIN1 and PIN3 protein abundance in *DN-rop3* and *rop3* mutant roots is due to altered *PIN* transcript level, we examined the RNA transcript of the *PIN1* and *PIN3* genes in wild-type, *DN-rop3*, and *rop3* roots. qRT-PCR analysis showed that the expression levels of *PIN1* and *PIN3* in *DN-rop3* and *rop3* mutant roots were not substantially different from the wild type (Supplemental Figure 7), suggesting that downregulation of PIN1 and PIN3 proteins in *DN-rop3* and *rop3* mutant roots occur at the posttranscriptional level.

Two other auxin transporters are not affected by *ROP3* mutations. PIN2:GFP, which localizes to the basal side of the root cortical cells and the apical side of the epidermis cells in the wild-type roots (Supplemental Figure 8A) did not change its

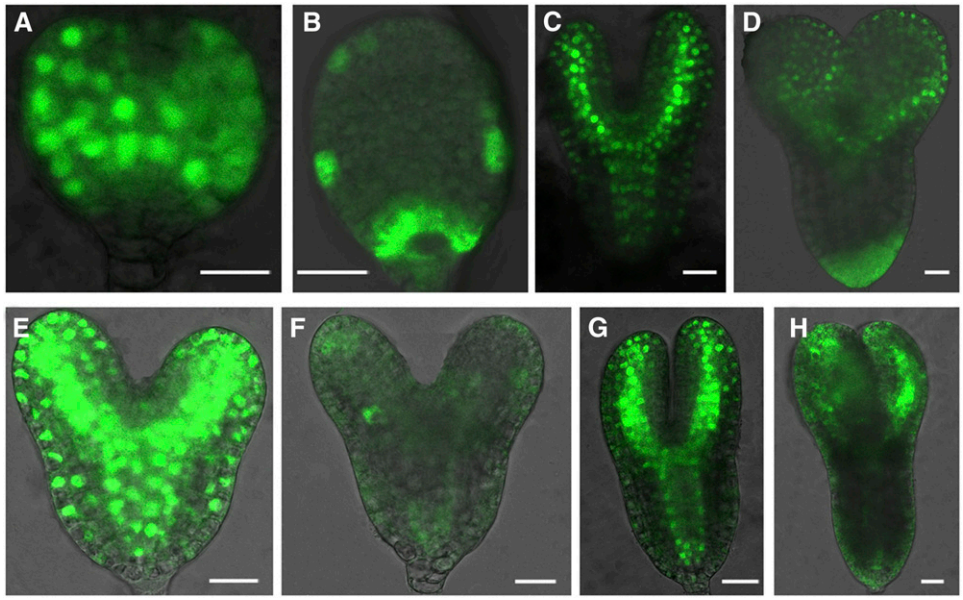


**Figure 7.** ROP3 Affects Embryonic Expression of *MP*.

**(A)** to **(D)** $MP_{pro}$*:3XGFP* is expressed in the wild type ([A] and [C]) and $RPS5A_{pro}$*:DN-rop3* ([B] and [D]) at triangle and torpedo stages, respectively.
**(E)** to **(H)** $MP_{pro}$*:3XGFP* is expressed in the wild type (**[E]** and **[G]**) and *rop3* (**[F]** and **[H]**) at heart and torpedo stages, respectively.
Bars = 20 μm.
[See online article for color version of this figure.]

polarity in *DN-rop3* and *rop3* mutant roots (Supplemental Figures 8B and 8C). The localization of auxin influx carrier AUX1-YFP, which is apically localized in the wild-type root protophloem cells (Figure 9P), is also not altered in *DN-rop3* and *rop3* mutants (Figures 9Q and 9R compared with 9P). We also confirmed that *ROP3* mutations had no effect on the transcript levels of *PIN2* and *AUX1* genes compared with the wild type (Supplemental Figure 7). These observations demonstrate that ROP3 specifically regulates the level and localization of PIN1 and PIN3 in the roots. Taken together, our data suggest that ROP3 regulates auxin distribution in embryos and seedling roots and that some *DN-rop3* and *rop3* phenotypes could have resulted from changes in PIN1 and PIN3 polarity or level.

### ROP3 Regulates the Recycling of PIN1 and PIN3 to the PM

PIN proteins continuously cycle between endosomes and the PM (Steinmann et al., 1999; Geldner et al., 2003). The reduced enrichment of PIN1 and PIN3 in the PM in *DN-rop3* and *rop3* mutants (Figure 9; Supplemental Figure 6) suggests that ROP3 is involved in the recruitment of PINs to the PM. To address this possibility, PIN1:GFP trafficking was investigated using brefeldin A (BFA), a vesicle trafficking inhibitor that inhibits PIN recycling and results in the formation of membrane protein aggregates referred to as BFA compartments (Geldner et al., 2001). BFA compartment formation was examined in the wild-type, *DN-rop3*, and *rop3* mutants. After BFA treatment (100 μM) for 1 h, similar levels (between 73.5 and 76.1%) of seedling root cells accumulated PIN1:GFP-containing BFA compartments in wild-type, *DN-rop3*, and *rop3* mutants (Figures 10A to 10C and 10M). The effects of BFA treatment on vesicle trafficking are reversible. After washout of BFA for 90 min, BFA compartments were still detected in 20.7 and 17.1% of root cells in *DN-rop3* and *rop3* mutants (Figures 10E and 10F), respectively, compared with in only 6.7% of wild-type root cells (Figures 10D and 10M). We next analyzed whether *ROP3* mutations affected the trafficking of PIN3:GFP and observed a similar result to PIN1:GFP for PIN3:GFP at BFA treatment (Figures 10G to 10I and 10N) and washout conditions (Figures 10J to 10L and 10N). However, PIN2:GFP recycling was not affected in wild-type, *DN-rop3*, or *rop3* roots (Supplemental Figures 10A to 10G). Additionally, the trafficking of a PM marker, water channel protein PIP2:GFP, was not impaired in *DN-rop3* and *rop3* mutants in contrast to the wild type (Supplemental Figures 11A to 11G), suggesting that ROP3 regulates recycling of specific PIN proteins but does not affect the trafficking of PIN2 and general PM proteins. Thus, it is likely that *DN-rop3* and *rop3* phenotypes are associated with alteration of auxin transport and PIN1 and PIN3 function.

### Inhibition of Proteasome Activity Enhances PIN1:GFP and PIN3:GFP Accumulation in *DN-rop3* and *rop3* Mutants

As ROP3 mutations do not interfere with the transcription of *PIN1* and *PIN3* (Supplemental Figure 7) but affect the recruitment of PIN1 and PIN3 to the PM (Supplemental Figures 6 and 10), it is likely that the reduced GFP-tagged PIN1 and PIN3 signals in *rop3* mutants are associated with protein degradation. We examined the PIN1:GFP and PIN3:GFP protein levels in *rop3* mutants by immunoblotting analysis and detected small, comparable amounts of PIN1:GFP in *DN-rop3* and *rop3* lines, in contrast to the larger amounts detected in the wild type (Figures 11A and 11B). The

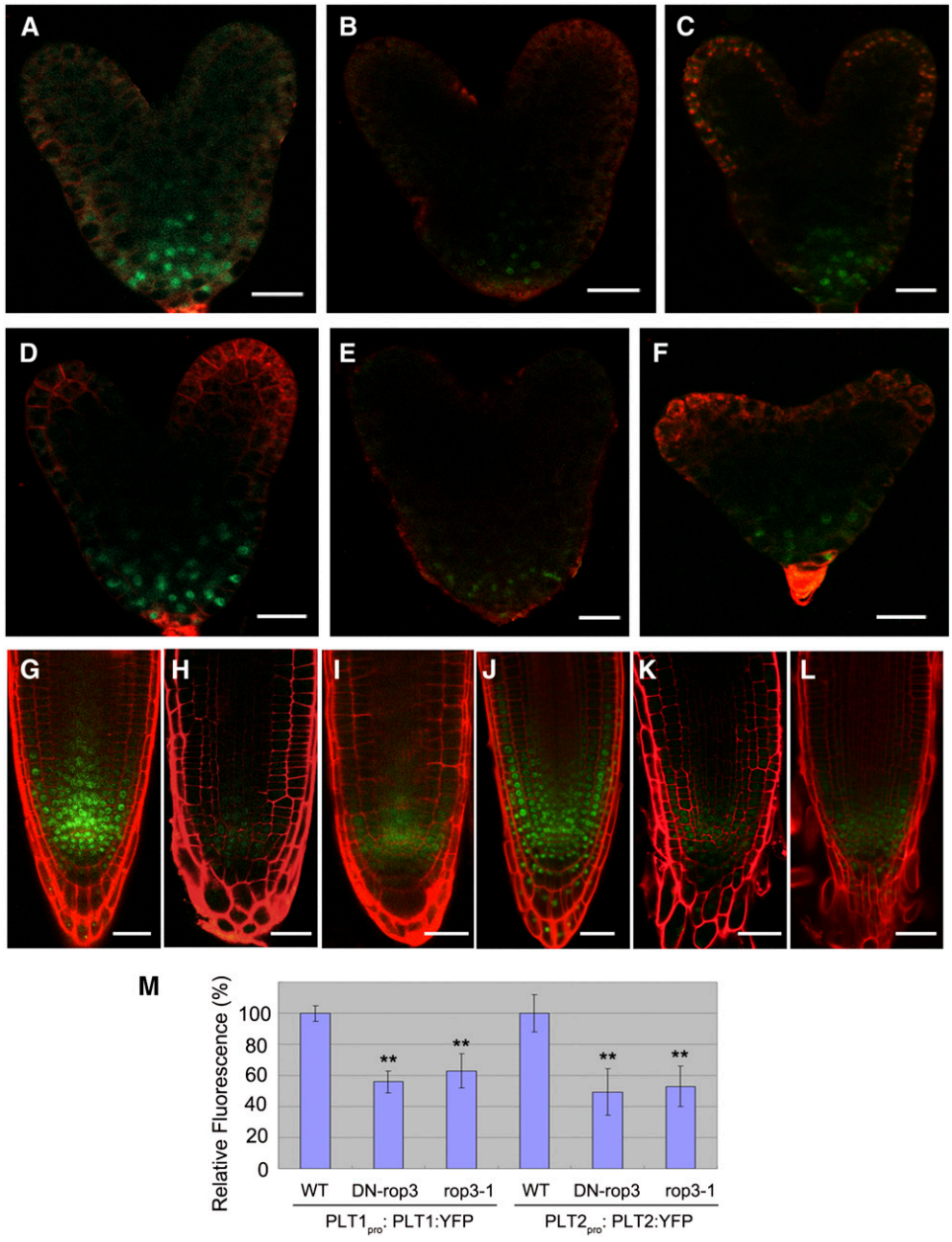


**Figure 8.** ROP3 Mutations Affect the Expression of *PLT1* and *PLT2*.

**(A)** to **(C)** The expression of PLT1 $_{pro}$:PLT1:YFP in embryos of the wild type **(A)**, *RPS5A*$_{pro}$*:DN- rop3* **(B)**, and *rop3* **(C)**.
**(D)** to **(F)** The expression of PLT2 $_{pro}$:PLT2:YFP in embryos of the wild type **(D)**, *RPS5A*$_{pro}$*:DN-rop3* **(E)**, and *rop3***(F)**.
**(G)** to **(I)** The expression of PLT1 $_{pro}$:PLT1:YFP in roots of the wild type **(G)**, *35S*$_{pro}$*:DN-rop3* **(H)**, and *rop3* **(I)**.
**(J)** to **(L)** The expression of PLT2 $_{pro}$:PLT2:YFP in roots of the wild type **(J)**, *35S*$_{pro}$*:DN-rop3* **(K)**, and *rop3* **(L)**.
**(M)** Quantification of PLT1$_{pro}$:PLT1:YFP and PLT2$_{pro}$:PLT2:YFP fluorescence intensity as shown in **(A)** to **(F)**. Data shown are average and SD ($n$ = 20 to 30). Asterisks indicate Student's $t$ test significant difference between the wild type and mutant embryos (**P < 0.01).
Bars = 20 μm.

PIN3:GFP level was affected more in *DN-rop3* mutants than in the *rop3* line. This observation might reflect that PIN1 accumulation is largely dependent on ROP3, whereas PIN3 accumulation is affected by ROP3 and also most probably by other ROPs. Figures 11A and 11B also showed that MG132-treated seedlings had an increase at PIN1:GFP and PIN3:GFP protein levels in wild-type, *DN-rop3*, and *rop3* compared with untreated controls. Since previous studies showed PIN proteins were targeted to vacuoles for degradation (Kleine-Vehn et al., 2008a), we therefore also examined the cellular fate of these PINs in *DN-rop3* and *rop3* seedlings

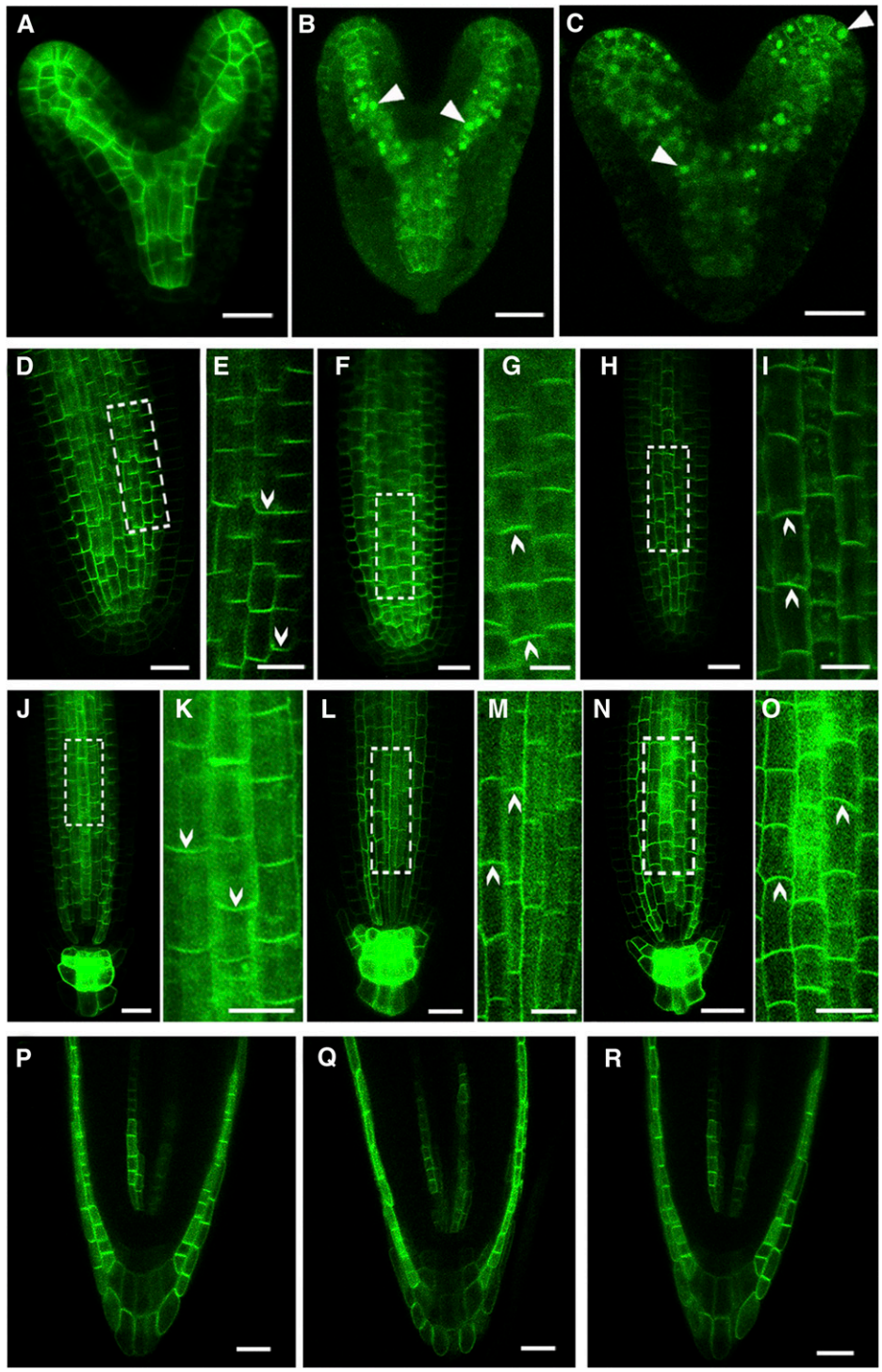


**Figure 9.** ROP3 Is Required for the Polar Localization of PINs.

**(A)** to **(C)** PIN1$_{pro}$:PIN1:GFP localization in embryos of the wild type **(A)**, *RPS5A$_{pro}$:DN-rop3* **(B)**, and *rop3* **(C)**. Arrowheads indicate intracellular aggregates of PIN1 protein.

**(D)** to **(I)** PIN1$_{pro}$:PIN1:GFP localization in roots of 4-d-old wild-type (**[D]** and **[E]**), *35S$_{pro}$:DN-rop3* (**[F]** and **[G]**), and *rop3* (**[H]** and **[I]**) seedling. Regions in white boxes **(D)**, **(F)**, and **(H)** are confocal scans with high magnifications shown in **(E)**, **(G)**, and **(I)**. Arrowheads indicate the direction of PIN1 polarity.

**(J)** to **(O)** PIN3 $_{pro}$:PIN3:GFP localization in roots of 4-d-old wild-type (**[J]** and **[K]**), *35S$_{pro}$:DN-rop3* (**[L]** and **[M]**), and *rop3* (**[N]** and **[O]**) seedling. Regions in white boxes (**[K]**, **[M]**, and **[O]**) are confocal scans at high magnification. Arrowheads indicate the direction of PIN3 polarity.

**(P)** to **(R)** AUX1$_{pro}$:AUX1:YFP localization in roots of 4-d-old wild-type **(P)**, *35S$_{pro}$:DN-rop3* **(Q)**, and *rop3* **(R)** seedling.

Bars = 20 μm.

[See online article for color version of this figure.]

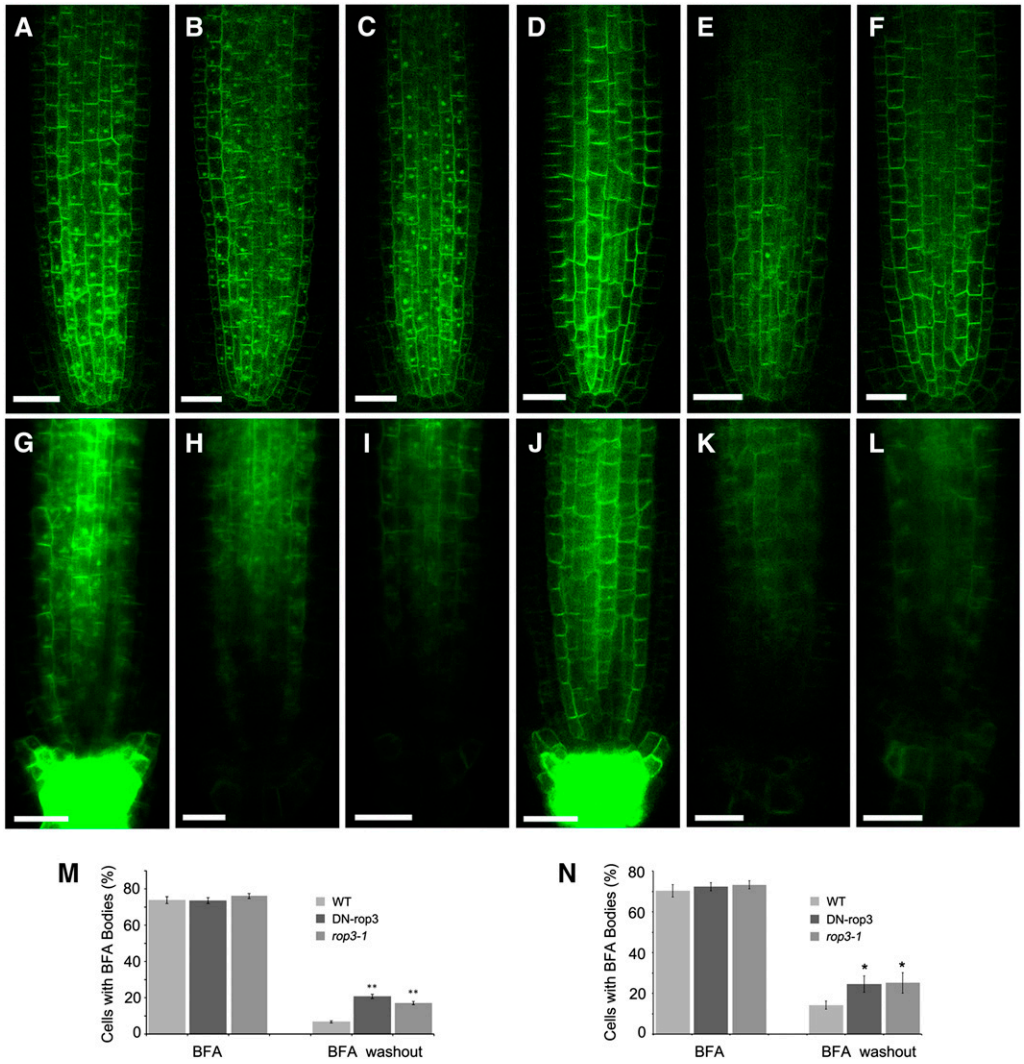


**Figure 10.** ROP3 Affects the Trafficking of PIN1:GFP and PIN3:GFP in Roots.

**(A)** to **(C)** BFA-treated seedlings expressing PIN1-GFP at 3 d after germination of the wild type **(A)**, *35S$_{pro}$:DN-rop3* **(B)**, and *rop3* **(C)**.
**(D)** to **(F)** BFA washout in PIN1:GFP **(D)**, *DN-rop3* **(E)**, and *rop3* **(F)**.
**(G)** to **(I)** BFA-treated seedlings expressing PIN3:GFP at 3 d after germination of the wild type **(G)**, 35S$_{pro}$:*DN-rop3* **(H)**, and *rop3* **(I)**.
**(J)** to **(L)** BFA washout in PIN3:GFP **(J)**, 35S$_{pro}$:*DN-rop3* **(K)**, and *rop3* **(L)**.
**(M)** and **(N)** Percentage of stele cells with PIN1:GFP-labeled **(M)** or PIN3:GFP-labeled **(N)** BFA bodies before and after BFA washout in the wild type, *35S$_{pro}$:DN-rop3*, and *rop3*. Data are means ± SD (*n* = cell numbers from 15 to 30 roots), and asterisks indicate significant differences by Student's *t* test (**P < 0.01; *P < 0.05). Bars = 20 μm.
[See online article for color version of this figure.]

using the fluorescent dye lysotracker red, which specifically marks acidic endomembrane compartments (Laxmi et al., 2008). In these MG132-treated seedling roots, we observed PIN1:GFP signal in circle-like structures that overlapped with the vacuoles labeled with lysotracker red in *DN-rop3* (22.2%, *n* = 36; Figure 11F) and *rop3* (16.2%, *n* = 37; Figure 11H) compared with none in the wild type (0%, *n* = 30; Figure 11D). The DMSO-treated control wild-type, *DN-rop3*, and *rop3* roots did not show vacuole-localized signal (Figures 11C, 11E, and 11G). These data suggest that changes in PIN1:GFP protein abundance in *rop3* mutants might associate with protein degradation that partially occur at the vacuoles. On the other hand, PIN3:GFP did not accumulate notably in the vacuoles of MG132-treated *rop3* mutants (Supplemental Figure 12).

## DISCUSSION

### ROP3 Regulates Auxin-Dependent Plant Development

ROP GTPases have been implicated in auxin signaling (Wu et al., 2011). However, details on the contributions of specific ROPs to auxin-regulated development has been sparse. The

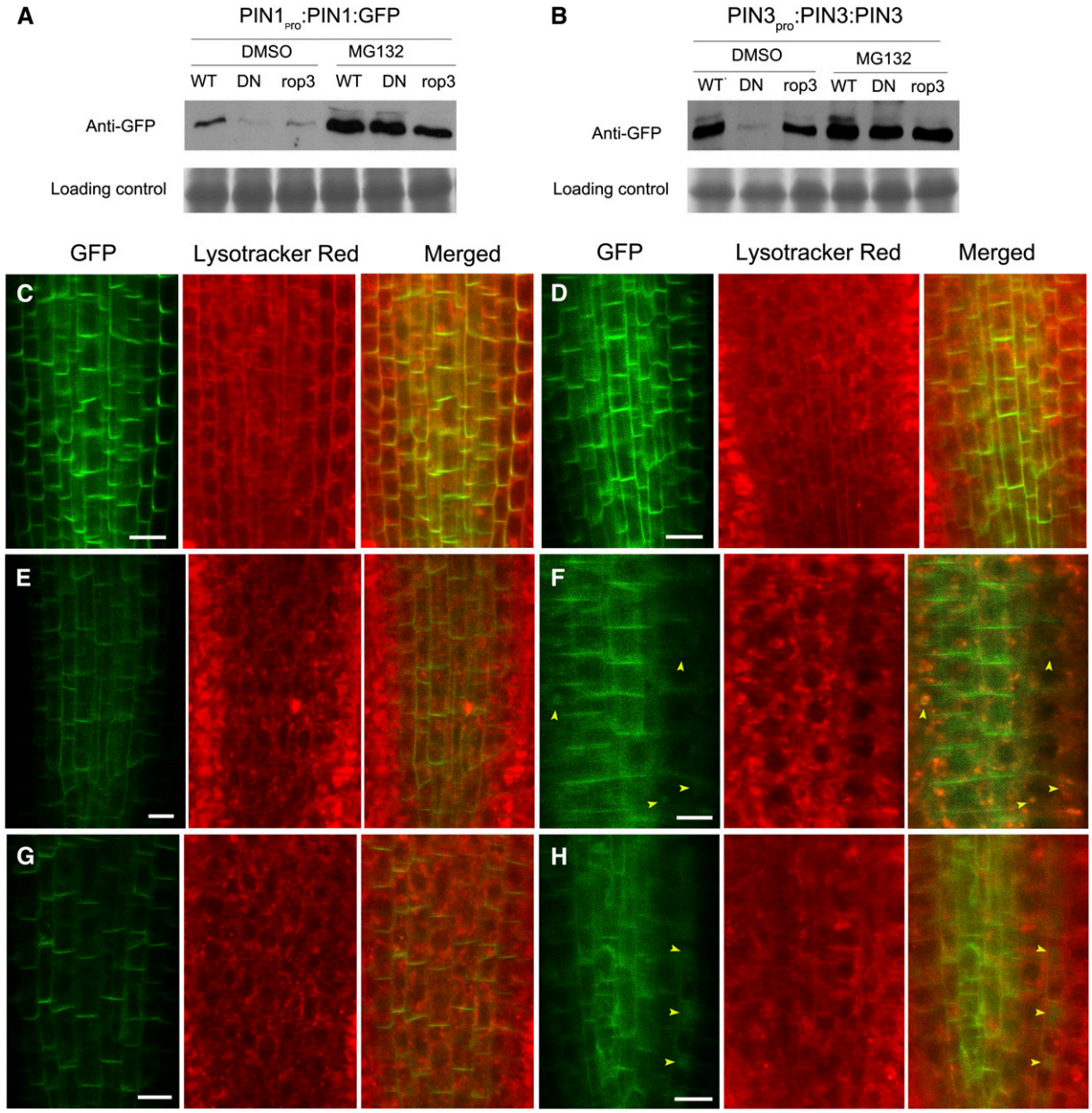


**Figure 11.** PIN1:GFP Partially Accumulates in Vacuoles in MG132-Treated Roots of 35S$_{pro}$:*DN-rop3* and *rop3*.

**(A)** and **(B)** PIN1: GFP **(A)** and PIN3:GFP **(B)** protein levels in MG132-treated and untreated wild-type, *DN-rop3*, and *rop3* seedlings. DN represents 35S$_{pro}$:*DN-rop3*. Immunoblot was performed using anti-GFP antibody. Lower panels indicate Coomassie blue staining of the protein samples as loading controls

**(C)** and **(D)** PIN1:GFP localization in roots of 5-d-old seedlings not treated **(C)** or treated with MG132 **(D)**.

**(E)** and **(F)** PIN1:GFP localization in roots of 35S$_{pro}$:*DN-rop3* seedlings not treated **(C)** or treated with MG132 **(D)**.

**(G)** and **(H)** PIN1:GFP localization in roots of *rop3* seedlings untreated **(E)** or treated with MG132 **(F)**.

Lysotracker red was used for labeling of vacuolar compartments. Arrowheads mark the vacuoles containing PIN1:GFP. Bars = 10 μm.

results presented here demonstrate that ROP3 plays a key role in auxin-regulated development throughout embryogenesis (Figures 2 and 3) and in postembryonic processes (Figures 4 and 5), including the gravitropic response (Figure 5A), auxin-suppressed root growth (Figure 5B), and sensitivity to auxin-regulated hypocotyl elongation at elevated temperature (Figure 5C). In showing that ROP3 is important for maintaining the *DR5rev:GFP*-marked auxin-responsive maxima (Figures 6A to 6F), the expression of MP/AUXIN RESPONSE FACTOR5 (ARF5) (Figures 7A to 7H) and PLT1/2 (Figures 8A to 8M), our results provide insights on the

cellular and physiological processes that underpin the developmental role of ROP3.

Taken together with the developmental phenotypes observed in *DN-rop3* and *rop3* mutants, the expression pattern of *ROP3* is consistent with this small GTPase being important in regulating auxin-mediated patterning during embryogenesis (Figures 2 and 3), organ formation, and seedling growth (Figures 4 and 5). The dynamic expression pattern of $ROP3_{pro}$*:GUS*, shifting from an apical to a basal high from early to developed embryos (Figure 1), strongly resembles changes in auxin distribution, as reflected by DR5rev:GFP accumulation during embryogenesis (Friml et al., 2003). ROP3 peak activity in the embryo and root (Figure 1) corresponds to the sites of auxin maxima in the hypophysis, quiescent center/columella initials, and cotyledon primordia, consistent with an important role for ROP3 in embryo development. Moreover, postembryonically, ROP3 expression (Figure 1; Supplemental Figure 1) overlapped with those of PIN1 and PIN3 in the root (Blilou et al., 2005; Vieten et al., 2005) and appeared similar to PIN3 in root columella cells (Blilou et al., 2005; Vieten et al., 2005). Furthermore, the failure of DN-rop3 to recruit PIN1 and PIN3 proteins to the PM in roots (Supplemental Figure 6) occurred along with diminished cell membrane localization, as suggested by the cytoplasmic and perinuclear localization of YFP:DN-rop3 (Supplemental Figures 1G and 1H). This observation is consistent with cell membrane association of ROP3 (Supplemental Figures 1E and 1F) being important for the recruitment of PINs to the PM. Taken together with PINs being the predominant auxin transporter in the stele, the ROP3 expression pattern is consistent with its involvement in the regulation of PIN-mediated auxin transport in the root, thereby regulating seedling development. Furthermore, the observation that *ROP3* expression in the root is enhanced in response to auxin induction (Figures 1I and 1J) is also consistent with ROP3 engaging in a regulatory loop responsive to auxin, augmenting its importance in auxin-mediated organogenesis and growth.

### ROP3 Functions in the Regulation of PIN Polarity and Trafficking

Several recent observations indicated a link between ROP function and PIN endocytosis (Chen et al., 2012; Lin et al., 2012; Nagawa et al., 2012). Our results (Figure 10) show that downregulating ROP signaling or loss of ROP3 function disrupts PIN1 and PIN3 recycling. Together, these results imply that different ROPs could perform distinct functions in the regulation of PIN trafficking, thereby leading to altered PIN polarity and perturbing directional auxin transport. Moreover, our results also show that ROP3 differentially affects auxin transporters, even within the PIN family (Figure 9; Supplemental Figure 8). On the other hand, despite overlapping with *AUX1* in its expression domain, *ROP3* has no impact on the polarity of AUX1 (Figures 9P to 9R). These data suggest that ROP3 specifically affects the localization of PIN proteins in regions of the root where they coexpress during development.

ROPs are activated by auxin (Tao et al., 2002; Xu et al., 2010) and activated ROPs interact with effectors, such as RIC1 and ICR1, that have been linked to auxin signaling. Among these ROP effectors, evidence convincingly supports that ICR1 regulates the exocytic trafficking of PIN proteins to polar domains in the PM and is required for auxin transport, most strongly impacting embryo and root meristem patterning (Hazak et al., 2010). On the other hand, phenotypes of downregulated *RIC1* mutants were relatively mild, e.g., only moderately enhanced lateral root development and weak defects in leaf vasculature were reported for *ric1* (Chen et al., 2012; Lin et al., 2012). It is therefore likely that ICR1 could act as a downstream effector of ROP3, mediating auxin-regulated responses. Future studies will be needed to elucidate whether ROP3 connects with the ICR1-dependent downstream pathway resulting in PIN polarization.

Another possible mechanism for how ROP3 might regulate the polarity of PIN proteins via PID. PID and related AGC kinases had been reported to promote transcytosis-directed apical PIN delivery through phosphorylation of PIN proteins (Dhonukshe et al., 2010). The activity of PID is stimulated by phospholipid signaling (Zegzouti et al., 2006). In pollen tubes, ROPs have been demonstrated to be associated with phosphatidylinositol monophosphate kinase (PtdIns p-K) activity (Kost et al., 1999). This might be mediated through their C-terminal polybasic domain, a feature common to RAS-related small GTPases and known to interact with both phosphatidylinositol 4,5-bis phosphate and phosphatidylinositol 3,4,5-triphosphate (Heo et al., 2006). Based on these observations, even if ROP-mediated PIN polarity might not directly target PID, it could provide a potential integration point for multiple cellular processes to influence auxin-dependent development through ROP signaling.

PIN protein abundance in the PM can be controlled by endocytosis or exocytosis (Löfke et al., 2013). Some PINs are targeted to the lytic vacuole in a retromer-dependent manner and degraded (Kleine-Vehn et al., 2008a). Our BFA treatment and washout experiments suggest that *ROP3* mutations specifically affect PIN1 and PIN3 recycling back to the PM (Figure 10; Supplemental Figures 10 and 11). The recycling defects of PIN1 and PIN3 in *rop3* mutants could apparently trigger protein degradation. Treatment with the 26S proteasome inhibitor MG132 enhances PIN1 protein accumulation at the cytoplasm and in the vacuoles (Figures 11C to 11F) in *DN-rop3* and *rop3* mutants. However, we could not find vacuolar accumulation of PIN3 in *DN-rop3* and *rop3* mutants (Supplemental Figure 12). At present, the precise mechanism on how ROP3 recruits PIN proteins is not known; we expect future studies of ROP3 downstream interacting proteins to shed light on its roles in the control of cell polarity of the polar auxin transport system.

How ROP3 activity is regulated so as to impact the auxin-related processes described here remains unknown. AUXIN BINDING PROTEIN1 (ABP1) has been suggested to act upstream of ROP6 and ROP2, which regulate PIN1 internalization and mediate the auxin signal to activate these small GTPases (Xu et al., 2010). ABP1 has also been shown to negatively regulate the auxin-controlled $SCF^{TIR1/AFB}$ pathway (Tromas et al., 2013). It therefore remains to be seen whether ABP1 is part of the ROP3-mediated signaling pathway.

Studies involving receptor-like kinases have provided support for a model whereby RopGEFs serve as linkages between cell surface signal perception and ROP activation (Kaothien et al., 2005; Nibau et al., 2006; Zhang and McCormick, 2007; Zhang et al., 2008; Duan et al., 2010; Nibau and Cheung, 2011). In these studies, two related pollen-specific receptor-like kinases from tomato (*Solanum lycopersicum*) and *Arabidopsis* have been shown to interact with RopGEFs, mediating similar ROP-induced

phenotypes in pollen tubes. Additionally, the FERONIA receptor kinase (FER) was identified as a regulator of auxin-stimulated NADPH oxidase-dependent reactive oxygen species-mediated root hair tip growth (Duan et al., 2010), an auxin- and ROP-regulated process (Foreman et al., 2003). FER interacts with RopGEFs, and RopGEF7 (Duan et al., 2010) regulates accumulation of PIN1 protein in embryonic and root cells and is required for the formation of auxin maxima (Chen et al., 2011). RopGEF7 is expressed in quiescent center cells and interacts with ROP3 (Chen et al., 2011) and both *RopGEF7* and *ROP3* are transcriptionally induced by auxin. Our results (Figure 1) show that ROP3 is also expressed in the hypophysis and its daughter cells. Therefore, FER, RopGEF7, and/or other members of these protein families that are expressed in the same tissue domain as ROP3 could act as upstream regulators of the ROP3-regulated processes described here. Future studies will decipher the mechanisms that underlie how the ROP3 switch is regulated.

## METHODS

### Plant Materials and Growth Conditions

*Arabidopsis thaliana* plants used in this study were Columbia-0 ecotype. The *DR5rev:GFP* (Benková et al., 2003), *PIN1*$_{pro}$*:PIN1:GFP* (Benková et al., 2003), *PIN2*$_{pro}$*:PIN2:GFP* (Blilou et al., 2005), *PIN3*$_{pro}$*:PIN3:GFP* (Blilou et al., 2005), *AUX1*$_{pro}$*:AUX1:YFP* (Swarup et al., 2004), *35S1*$_{pro}$*: PIP2:GFP* (Cutler et al., 2000), *PLT1* $_{pro}$*:PLT1:YFP*, *PLT2*$_{pro}$*:PLT2:YFP* (Grieneisen et al., 2007), and *MP*$_{pro}$*:n3xGFP* (Rademacher et al., 2012) constructs have been described previously.

Seeds were surface-sterilized and plated on half-strength Murashige and Skoog (MS) medium containing 1.5% sucrose and 0.8% agar. Seeds on one-half MS plates were stratified at 4°C for 2 to 3 d in darkness and transferred to a phytotron set with a 16-h-light/8-h-dark cycle at 22°C. After 7 to 10 d, seedlings were transferred to soil and grown under the same conditions.

### Vector Construction and Plant Transformation

*ROP3*$_{pro}$*:GUS* was generated by insertion of a 1.034-kb PCR-amplified *ROP3* promoter sequence into pBI101.1 at the *Sal*I and *Bam*HI sites. *DN-rop3* mutation with an A121D conversion in ROP3 was created by site-specific mutagenesis of the *ROP3* cDNA subcloned in a Bluescript pSK vector. The mutant version of *ROP3* (*DN-rop3*) was then cloned into the pAC1352 binary vector carrying cauliflower mosaic virus *35S* promoter and a modified pCambia1300 containing the embryo-specific *RPS5A* promoter, which have been previously described (Chen et al., 2011).

The above constructs were introduced into *Agrobacterium tumefaciens* strain C58, which were used for transformation of *Arabidopsis* by the floral dip method (Clough and Bent, 1998). The sequences of the primers used in the vector construction are listed in Supplemental Table 1.

### Identification of *rop3* Mutants and Complementation of *ROP3*

Two *Arabidopsis* T-DNA insertion lines for *rop3-1* (SALK_008896) and *rop3-2* (SALK_032558C) were obtained from ABRC. A PCR-based approach was used to confirm the T-DNA insertion and to identify the homozygous lines. Transcript levels in mutants and wild-type plants were analyzed by qRT-PCR analysis. Primers used for the identification of the mutants are listed in Supplemental Table 1.

The *ROP3* promoter was subcloned into a modified *PBI101* vector to generate *ROP3*$_{pro}$*:ROP3* harboring cDNA of *ROP3*. The construct was transformed into wild-type plants and homozygous lines were crossed with *rop3* mutants for complementation studies. Transcript levels of *ROP3* in *rop3* mutants were confirmed by qRT-PCR.

### NAA Treatment

Wild-type seeds were surface sterilized and germinated on half-strength MS agar plates. Five- to seven-day-old seedlings were treated with 10 μM NAA for 0, 6, 12, and 24 h, respectively, and roots were harvested for RNA extraction. Expression levels of *ROP3* were analyzed by qRT-PCR.

### qRT-PCR Analysis

For analysis of *ROP3* gene expression, total RNA was extracted from embryos and 7- to 10-day-old seedlings using the RNeasy plant mini kit (Qiagen). For the analysis of *PIN1*, *PIN2*, *PIN3*, and *AUX1* transcripts in wild-type, *DN-rop3*, and *rop3* mutant plants, root samples from 7-d-old seedlings were collected and subjected to total RNA extraction. Root longitudinal section preparation and RNA extraction were performed as described by Dinneny et al. (2008) with some modifications. Roots of 5-d-old seedlings were cut into three regions using a scalpel. The first cut was made ~350 μm from the root tip at the point of the end of the meristematic zone (Zone 1); the second cut was made ~200 to 300μm above the first cut, below the region where root hairs emerge (Zone 2-elongation zone); the third cut was made ~1 mm above the second cut (Zone 3-maturation zone). Forty roots were collected per replicate. Two replicates were performed per zone. RNA was extracted using the RNAprep Pure Micro Kit (Tiangen).

cDNA was prepared from 3 μg of total RNA with PrimeScript reverse transcriptase (TakaRa). PCR reaction was performed on an Illumina Eco (Illumina) system with a SYBR probe (TAKARA). Expression of *ROP3*, *PIN1*, *PIN2*, *PIN3*, and *AUX1* in transgenic or mutant plants were normalized to the expression of *ACTIN2* and then compared with the wild type. Data presented are the averages from at least three biological replicates with SD.

A list of gene-specific primers used is provided in Supplemental Table 1.

### Immunoblot Analysis

Embryos and 7-d-old wild-type seedlings and seedlings containing *RPS5A*$_{pro}$*: DN-rop3* and *35S*$_{pro}$*:DN-rop3* constructs, respectively, were collected for total protein extraction. Anti-ROP3 antibody (Abmart) was used for the detection of ROP3. For PIN1:GFP and PIN3:GFP fusion proteins, anti-GFP antibody (Abcam) was used for the detection of GFP-tagged fusion proteins. Coomassie Brilliant Blue-stained protein samples are shown as loading controls.

### Phenotypic Analysis of Transgenic Plants, Mutants, and Gravity Response

Seedlings of wild-type, transgenic plants and mutants were grown on half-strength MS medium containing 1.5% sucrose and 0.8% agar for 4 d, then transferred to medium supplemented with different concentrations of NAA (0, 50, 75, and 100 nM and 1 μM) for another 5 d, and the primary root length was measured. For hypocotyl elongation analysis, seedlings were grown at 22 or 29°C in the vertical position for 7 d, and hypocotyl lengths were measured. The root gravity response was determined using 4-d-old seedlings. The angle of root curvature was measured at 2, 4, 8, 12, and 24 h after a 90° reorientation. The above measurements were performed with the aid of the image analysis software Image J (version 1.47; http://rsb.info.nih.gov/ij). Thirty to fifty seedlings were used for measurement, and data presented are the averages of 30 to 50 seedlings with SD. The statistical significance was evaluated by Student's *t* test analysis. For multiple comparisons, an analysis of variance followed by Dunnett's LSD

method was performed on the data. Single and double asterisks indicate significant differences from control at the level of $P < 0.05$ and $P < 0.01$, respectively.

### Pollen Phenotype Analysis of *rop3* Mutants

Freshly anther-dehisced flowers were used for pollen viability assays and in vivo pollen germination experiments. Pollen grains from the dehisced anthers of randomly picked flowers were dipped in the Alexander and 4′,6-diamidino-2-phenylindole solution droplets on slides and observed by differential interference contrast and fluorescence microscopy, respectively. The limited pollination experiments were performed as described by Chen et al. (2007). Stage 12 flowers were emasculated and pollinated by 10 to 30 pollen grains from wild-type and *rop3* mutant plants 12 h after emasculation. Pistils were collected 2 h after pollination. Aniline blue staining of pollen tubes was performed as described by Chen et al. (2007).

### Marker Gene Analysis

DR5rev:GFP, $PIN1_{pro}$:PIN1:GFP, $PIN2_{pro}$:PIN2:GFP, $PIN3_{pro}$:PIN3:GFP, $AUX1_{pro}$:AUX1:YFP, $PLT1_{pro}$:PLT1:YFP, $PLT2_{pro}$:PLT2:YFP, and $Mp_{pro}$:n3xGFP were individually crossed into rop3-1 and the strongest transgenic line of DN-rop3. Homozygous plants were isolated from F2 populations. These homozygotes in F3 and later generations were used for analyses.

### BFA Treatment and Washout Analysis

Three-day-old seedlings were incubated in half-strength MS medium containing 100 μM BFA (Sigma-Aldrich) for 40 min and observed or washed with half-strength MS medium for 90 min. For quantitative analysis of BFA bodies, stele cells from 15 to 30 roots were used for each assay.

### MG132 Treatment and Lysotracker Red Labeling

Five-day-old seedlings were incubated with 50 μM MG132 (Sigma-Aldrich) for 4 h in darkness, and DMSO incubation was used as the control. Lysotracker red (2 μM; Invitrogen) was applied on seedlings for 1 h before confocal imaging analysis.

### Microscopy

Ovules and seedling roots were cleared in a Hoyer's solution and an HCG (water, chloral hydrate, and glycerol-containing) solution as previously described (Chen et al., 2011). For Lugol staining of roots, root tips were incubated in a 1:1 dilution of Lugol's solution (Sigma-Aldrich) for 1 min, then washed with water and mounted in the HCG solution for microscopy analysis. Histochemical staining for GUS activity was performed as previously described (Chen et al., 2011). Embryos, different tissues, and seedlings were incubated in GUS (0.5 mg/mL) staining buffer from 6 to 36 h at 37°C. Differential interference contrast imaging was performed on an Olympus BX51 microscope equipped with a Ritiga 2000R camera. Seedlings were photographed under a Nikon SMZ1000 microscope using a Nikon digital sight Ds-Fi1 camera.

Dissected embryos and seedlings were stained with 1 μg/mL FM4-64 and 100 μg/mL propidium iodide for confocal microscopy. GFP, YFP, FM4-64, and propidium iodide fluorescence were imaged under SP2 Leica confocal laser scanning microscope. The fluorescent markers were visualized with the following excitation (Ex) and emission (Em) wavelengths (Ex/Em): 488 nm/505 to 530 nm for GFP, 514 nm/530 to 560 nm for YFP, 543 nm/600 nm for FM4-64, and 561 nm/591 to 635 nm for propidium iodide.

Twenty to thirty samples for each line were first analyzed under the Olympus BX51 microscope and then 10 to 15 samples were used for confocal imaging. Each experiment was repeated three to four times with similar results.

### Accession Numbers

Sequence data from this article can be found in the Arabidopsis Genome Initiative or GenBank/EMBL databases under the following accession numbers: *ACTIN2* (At3g18780), *PIN1* (At1g73590), *PIN2* (At5g57090), *PIN3* (At1g70940), *AUX1* (At2g38120), *PIP2* (At3g53420), *MP* (At1g19850), *PLT1* (At3g20840), *PLT2* (At1g51190), *RopGEF7*(At5g02010), and *ROP3* (At2g17800).

### Supplemental Data

The following materials are available in the online version of the article.

**Supplemental Figure 1.** Analysis of *ROP3* Expression Pattern and Subcellular Localization.

**Supplemental Figure 2.** qRT-PCR Analysis of *DN-rop3* Transcripts and Immunoblot Analysis of DN-rop3 Protein Levels in the *DN-rop3* Transgenic Lines.

**Supplemental Figure 3.** Identification of the *rop3* T-DNA Insertion Mutants.

**Supplemental Figure 4.** The $ROP3_{pro}$*:ROP3* Transgene Rescues the Phenotypes in *rop3* Mutants.

**Supplemental Figure 5.** Pollen Development in *rop3* Mutants Is Normal.

**Supplemental Figure 6.** ROP3 Is Required for the Accumulation of $PIN1_{pro}$:PIN1:GFP and $PIN3_{pro}$:PIN3:GFP.

**Supplemental Figure 7.** ROP3 Has No Effect on the Transcript Levels of *PINs* and *AUX1* Genes.

**Supplemental Figure 8.** ROP3 Does Not Affect the Localization of PIN2:GFP.

**Supplemental Figure 9.** RopGEF7 Does Not Affect the Polarity of PIN1 and PIN3.

**Supplemental Figure 10.** ROP3 Does Not Affect the Trafficking of PIN2:GFP in Roots.

**Supplemental Figure 11.** ROP3 Does Not Affect the Trafficking of PIP2:GFP in Roots.

**Supplemental Figure 12.** PIN3:GFP Does Not Accumulate in Vacuole Compartments in MG132-Treated Roots of *DN-rop3* and *rop3.*

**Supplemental Table 1.** Primers Used in This Study.

**Supplemental Table 2.** Quantitative Analysis of *DN-rop3* and *rop3* Embryonic Phenotypes.

**Supplemental Table 3.** Quantitative Analysis of *DN-rop3* and *rop3* Seedling Phenotypes.

**Supplemental Table 4.** Quantitative Analysis of Embryo Phenotypes in the $ROP3_{pro}$*:ROP3* Transgene Rescued *rop3* Background.

## ACKNOWLEDGMENTS

We thank the ABRC (Ohio State University) and Ben Scheres, Chuanyou Li, Dolf Weijers, Jianwei Pan, and Malcolm Bennett for providing seeds used in this study. We thank Hen-ming Wu for critical reading and suggestions for the article. We thank Weicai Yang and Yanjiao Zou for sharing the protocols for pollen assays with us. This work was supported by grants from National Natural Science Foundation of China (91117007 and 31370312) and the Ministry of Science and Technology of China

(2007CB948200). J.X. was supported by the Ministry of Education of Singapore Academic Research Fund (Tier 2; MOE2012-T2-1-157).

## AUTHOR CONTRIBUTIONS

J.-b.H., H.L., M.C., J.X., A.Y.C., and L.-z.T. designed the research. J.-b.H., H.L., M.C., X.L., M.W., Y.Y., C.W., J.H., G.L., and Y.L. performed the experiments. J.-b.H., H.L., M.C., J.X., A.Y.C., and L.-z.T. analyzed the data. L.-z.T. wrote the article. A.Y.C., J.X., and L.-z.T. revised the article.

Received June 19, 2014; revised August 12, 2014; accepted August 22, 2014; published September 12, 2014.

## REFERENCES

**Aida, M., Beis, D., Heidstra, R., Willemsen, V., Blilou, I., Galinha, C., Nussaume, L., Noh, Y.S., Amasino, R., and Scheres, B.** (2004). The PLETHORA genes mediate patterning of the Arabidopsis root stem cell niche. Cell **119:** 109–120.

**Benková, E., Michniewicz, M., Sauer, M., Teichmann, T., Seifertová, D., Jürgens, G., and Friml, J.** (2003). Local, efflux-dependent auxin gradients as a common module for plant organ formation. Cell **115:** 591–602.

**Bennett, M.J., Marchant, A., Green, H.G., May, S.T., Ward, S.P., Millner, P.A., Walker, A.R., Schulz, B., and Feldmann, K.A.** (1996). Arabidopsis AUX1 gene: a permease-like regulator of root gravitropism. Science **273:** 948–950.

**Berken, A., Thomas, C., and Wittinghofer, A.** (2005). A new family of RhoGEFs activates the Rop molecular switch in plants. Nature **436:** 1176–1180.

**Blilou, I., Xu, J., Wildwater, M., Willemsen, V., Paponov, I., Friml, J., Heidstra, R., Aida, M., Palme, K., and Scheres, B.** (2005). The PIN auxin efflux facilitator network controls growth and patterning in Arabidopsis roots. Nature **433:** 39–44.

**Chen, M., Liu, H., Kong, J., Yang, Y., Zhang, N., Li, R., Yue, J., Huang, J., Li, C., Cheung, A.Y., and Tao, L.Z.** (2011). RopGEF7 regulates PLETHORA-dependent maintenance of the root stem cell niche in Arabidopsis. Plant Cell **23:** 2880–2894.

**Chen, X., Naramoto, S., Robert, S., Tejos, R., Löfke, C., Lin, D., Yang, Z., and Friml, J.** (2012). ABP1 and ROP6 GTPase signaling regulate clathrin-mediated endocytosis in Arabidopsis roots. Curr. Biol. **22:** 1326–1332.

**Chen, Y.H., Li, H.J., Shi, D.Q., Yuan, L., Liu, J., Sreenivasan, R., Baskar, R., Grossniklaus, U., and Yang, W.C.** (2007). The central cell plays a critical role in pollen tube guidance in Arabidopsis. Plant Cell **19:** 3563–3577.

**Christensen, S.K., Dagenais, N., Chory, J., and Weigel, D.** (2000). Regulation of auxin response by the protein kinase PINOID. Cell **100:** 469–478.

**Clough, S.J., and Bent, A.F.** (1998). Floral dip: a simplified method for Agrobacterium-mediated transformation of *Arabidopsis thaliana*. Plant J. **16:** 735–743.

**Craddock, C., Lavagi, I., and Yang, Z.** (2012). New insights into Rho signaling from plant ROP/Rac GTPases. Trends Cell Biol. **22:** 492–501.

**Cutler, S.R., Ehrhardt, D.W., Griffitts, J.S., and Somerville, C.R.** (2000). Random GFP:cDNA fusions enable visualization of subcellular structures in cells of Arabidopsis at a high frequency. Proc. Natl. Acad. Sci. USA **97:** 3718–3723.

**Dhonukshe, P., Huang, F., Galvan-Ampudia, C.S., Mähönen, A.P., Kleine-Vehn, J., Xu, J., Quint, A., Prasad, K., Friml, J., Scheres, B., and Offringa, R.** (2010). Plasma membrane-bound AGC3 kinases phosphorylate PIN auxin carriers at TPRXS(N/S) motifs to direct apical PIN recycling. Development **137:** 3245–3255.

**Dinneny, J.R., Long, T.A., Wang, J.Y., Jung, J.W., Mace, D., Pointer, S., Barron, C., Brady, S.M., Schiefelbein, J., and Benfey, P.N.** (2008). Cell identity mediates the response of Arabidopsis roots to abiotic stress. Science **320:** 942–945.

**Duan, Q., Kita, D., Li, C., Cheung, A.Y., and Wu, H.M.** (2010). FERONIA receptor-like kinase regulates RHO GTPase signaling of root hair development. Proc. Natl. Acad. Sci. USA **107:** 17821–17826.

**Feig, L.A.** (1999). Tools of the trade: use of dominant-inhibitory mutants of Ras-family GTPases. Nat. Cell Biol. **1:** E25–E27.

**Foreman, J., Demidchik, V., Bothwell, J.H., Mylona, P., Miedema, H., Torres, M.A., Linstead, P., Costa, S., Brownlee, C., Jones, J.D., Davies, J.M., and Dolan, L.** (2003). Reactive oxygen species produced by NADPH oxidase regulate plant cell growth. Nature **422:** 442–446.

**Friml, J., Vieten, A., Sauer, M., Weijers, D., Schwarz, H., Hamann, T., Offringa, R., and Jürgens, G.** (2003). Efflux-dependent auxin gradients establish the apical-basal axis of Arabidopsis. Nature **426:** 147–153.

**Friml, J., Wiśniewska, J., Benková, E., Mendgen, K., and Palme, K.** (2002). Lateral relocation of auxin efflux regulator PIN3 mediates tropism in Arabidopsis. Nature **415:** 806–809.

**Friml, J., et al.** (2004). A PINOID-dependent binary switch in apical-basal PIN polar targeting directs auxin efflux. Science **306:** 862–865.

**Galinha, C., Hofhuis, H., Luijten, M., Willemsen, V., Blilou, I., Heidstra, R., and Scheres, B.** (2007). PLETHORA proteins as dose-dependent master regulators of Arabidopsis root development. Nature **449:** 1053–1057.

**Geldner, N., Anders, N., Wolters, H., Keicher, J., Kornberger, W., Muller, P., Delbarre, A., Ueda, T., Nakano, A., and Jürgens, G.** (2003). The Arabidopsis GNOM ARF-GEF mediates endosomal recycling, auxin transport, and auxin-dependent plant growth. Cell **112:** 219–230.

**Geldner, N., Friml, J., Stierhof, Y.D., Jürgens, G., and Palme, K.** (2001). Auxin transport inhibitors block PIN1 cycling and vesicle trafficking. Nature **413:** 425–428.

**Gray, W.M., Ostin, A., Sandberg, G., Romano, C.P., and Estelle, M.** (1998). High temperature promotes auxin-mediated hypocotyl elongation in Arabidopsis. Proc. Natl. Acad. Sci. USA **95:** 7197–7202.

**Grieneisen, V.A., Xu, J., Marée, A.F., Hogeweg, P., and Scheres, B.** (2007). Auxin transport is sufficient to generate a maximum and gradient guiding root growth. Nature **449:** 1008–1013.

**Gu, Y., Vernoud, V., Fu, Y., and Yang, Z.** (2003). ROP GTPase regulation of pollen tube growth through the dynamics of tip-localized F-actin. J. Exp. Bot. **54:** 93–101.

**Hazak, O., Bloch, D., Poraty, L., Sternberg, H., Zhang, J., Friml, J., and Yalovsky, S.** (2010). A rho scaffold integrates the secretory system with feedback mechanisms in regulation of auxin distribution. PLoS Biol. **8:** e1000282.

**Heo, W.D., Inoue, T., Park, W.S., Kim, M.L., Park, B.O., Wandless, T.J., and Meyer, T.** (2006). PI(3,4,5)P3 and PI(4,5)P2 lipids target proteins with polybasic clusters to the plasma membrane. Science **314:** 1458–1461.

**Jaillais, Y., Santambrogio, M., Rozier, F., Fobis-Loisy, I., Miège, C., and Gaude, T.** (2007). The retromer protein VPS29 links cell polarity and organ initiation in plants. Cell **130:** 1057–1070.

**Kaothien, P., Ok, S.H., Shuai, B., Wengier, D., Cotter, R., Kelley, D., Kiriakopolos, S., Muschietti, J., and McCormick, S.** (2005). Kinase partner protein interacts with the LePRK1 and LePRK2 receptor kinases and plays a role in polarized pollen tube growth. Plant J. **42:** 492–503.

**Kleine-Vehn, J., Dhonukshe, P., Sauer, M., Brewer, P.B., Wiśniewska, J., Paciorek, T., Benková, E., and Friml, J.** (2008b). ARF GEF-dependent transcytosis and polar delivery of PIN auxin carriers in Arabidopsis. Curr. Biol. **18:** 526–531.

**Kleine-Vehn, J., Leitner, J., Zwiewka, M., Sauer, M., Abas, L., Luschnig, C., and Friml, J.** (2008a). Differential degradation of PIN2 auxin efflux carrier by retromer-dependent vacuolar targeting. Proc. Natl. Acad. Sci. USA **105:** 17812–17817.

**Kost, B., Lemichez, E., Spielhofer, P., Hong, Y., Tolias, K., Carpenter, C., and Chua, N.H.** (1999). Rac homologues and compartmentalized phosphatidylinositol 4, 5-bisphosphate act in a common pathway to regulate polar pollen tube growth. J. Cell Biol. **145:** 317–330.

**Lau, S., Slane, D., Herud, O., Kong, J., and Jürgens, G.** (2012). Early embryogenesis in flowering plants: setting up the basic body pattern. Annu. Rev. Plant Biol. **63:** 483–506.

**Laxmi, A., Pan, J., Morsy, M., and Chen, R.** (2008). Light plays an essential role in intracellular distribution of auxin efflux carrier PIN2 in *Arabidopsis thaliana*. PLoS ONE **3:** e1510.

**Li, H., Lin, Y., Heath, R.M., Zhu, M.X., and Yang, Z.** (1999). Control of pollen tube tip growth by a Rop GTPase-dependent pathway that leads to tip-localized calcium influx. Plant Cell **11:** 1731–1742.

**Lin, D., et al.** (2012). A ROP GTPase-dependent auxin signaling pathway regulates the subcellular distribution of PIN2 in Arabidopsis roots. Curr. Biol. **22:** 1319–1325.

**Löfke, C., Luschnig, C., and Kleine-Vehn, J.** (2013). Posttranslational modification and trafficking of PIN auxin efflux carriers. Mech. Dev. **130:** 82–94.

**Michniewicz, M., et al.** (2007). Antagonistic regulation of PIN phosphorylation by PP2A and PINOID directs auxin flux. Cell **130:** 1044–1056.

**Nagawa, S., Xu, T., Lin, D., Dhonukshe, P., Zhang, X., Friml, J., Scheres, B., Fu, Y., and Yang, Z.** (2012). ROP GTPase-dependent actin microfilaments promote PIN1 polarization by localized inhibition of clathrin-dependent endocytosis. PLoS Biol. **10:** e1001299.

**Nibau, C., and Cheung, A.Y.** (2011). New insights into the functional roles of CrRLKs in the control of plant cell growth and development. Plant Signal. Behav. **6:** 655–659.

**Nibau, C., Wu, H.M., and Cheung, A.Y.** (2006). RAC/ROP GTPases: 'hubs' for signal integration and diversification in plants. Trends Plant Sci. **11:** 309–315.

**Petricka, J.J., Winter, C.M., and Benfey, P.N.** (2012). Control of Arabidopsis root development. Annu. Rev. Plant Biol. **63:** 563–590.

**Rademacher, E.H., Lokerse, A.S., Schlereth, A., Llavata-Peris, C.I., Bayer, M., Kientz, M., Freire Rios, A., Borst, J.W., Lukowitz, W., Jürgens, G., and Weijers, D.** (2012). Different auxin response machineries control distinct cell fates in the early plant embryo. Dev. Cell **22:** 211–222.

**Steinmann, T., Geldner, N., Grebe, M., Mangold, S., Jackson, C.L., Paris, S., Gälweiler, L., Palme, K., and Jürgens, G.** (1999). Coordinated polar localization of auxin efflux carrier PIN1 by GNOM ARF GEF. Science **286:** 316–318.

**Swarup, K., et al.** (2008). The auxin influx carrier LAX3 promotes lateral root emergence. Nat. Cell Biol. **10:** 946–954.

**Swarup, R., et al.** (2004). Structure-function analysis of the presumptive Arabidopsis auxin permease AUX1. Plant Cell **16:** 3069–3083.

**Tao, L.Z., Cheung, A.Y., and Wu, H.M.** (2002). Plant Rac-like GTPases are activated by auxin and mediate auxin-responsive gene expression. Plant Cell **14:** 2745–2760.

**Tao, L.Z., Cheung, A.Y., Nibau, C., and Wu, H.M.** (2005). RAC GTPases in tobacco and Arabidopsis mediate auxin-induced formation of proteolytically active nuclear protein bodies that contain AUX/IAA proteins. Plant Cell **17:** 2369–2383.

**Tromas, A., Paque, S., Stierlé, V., Quettier, A.L., Muller, P., Lechner, E., Genschik, P., and Perrot-Rechenmann, C.** (2013). Auxin-binding protein 1 is a negative regulator of the SCF(TIR1/AFB) pathway. Nat. Commun. **4:** 2496.

**Vieten, A., Vanneste, S., Wisniewska, J., Benková, E., Benjamins, R., Beeckman, T., Luschnig, C., and Friml, J.** (2005). Functional redundancy of PIN proteins is accompanied by auxin-dependent cross-regulation of PIN expression. Development **132:** 4521–4531.

**Weijers, D., Franke-van Dijk, M., Vencken, R.J., Quint, A., Hooykaas, P., and Offringa, R.** (2001). An Arabidopsis Minute-like phenotype caused by a semi-dominant mutation in a RIBOSOMAL PROTEIN S5 gene. Development **128:** 4289–4299.

**Wisniewska, J., Xu, J., Seifertová, D., Brewer, P.B., Ruzicka, K., Blilou, I., Rouquié, D., Benková, E., Scheres, B., and Friml, J.** (2006). Polar PIN localization directs auxin flow in plants. Science **312:** 883.

**Wu, H.M., Hazak, O., Cheung, A.Y., and Yalovsky, S.** (2011). RAC/ROP GTPases and auxin signaling. Plant Cell **23:** 1208–1218.

**Xu, T., Wen, M., Nagawa, S., Fu, Y., Chen, J.G., Wu, M.J., Perrot-Rechenmann, C., Friml, J., Jones, A.M., and Yang, Z.** (2010). Cell surface- and rho GTPase-based auxin signaling controls cellular interdigitation in Arabidopsis. Cell **143:** 99–110.

**Yalovsky, S., Bloch, D., Sorek, N., and Kost, B.** (2008). Regulation of membrane trafficking, cytoskeleton dynamics, and cell polarity by ROP/RAC GTPases. Plant Physiol. **147:** 1527–1543.

**Yang, Z.** (2002). Small GTPases: versatile signaling switches in plants. Plant Cell **14** (suppl.): S375–S388.

**Yang, Z., and Fu, Y.** (2007). ROP/RAC GTPase signaling. Curr. Opin. Plant Biol. **10:** 490–494.

**Zegzouti, H., Anthony, R.G., Jahchan, N., Bögre, L., and Christensen, S.K.** (2006). Phosphorylation and activation of PINOID by the phospholipid signaling kinase 3-phosphoinositide-dependent protein kinase 1 (PDK1) in Arabidopsis. Proc. Natl. Acad. Sci. USA **103:** 6404–6409.

**Zhang, D., Wengier, D., Shuai, B., Gui, C.P., Muschietti, J., McCormick, S., and Tang, W.H.** (2008). The pollen receptor kinase LePRK2 mediates growth-promoting signals and positively regulates pollen germination and tube growth. Plant Physiol. **148:** 1368–1379.

**Zhang, Y., and McCormick, S.** (2007). A distinct mechanism regulating a pollen-specific guanine nucleotide exchange factor for the small GTPase Rop in *Arabidopsis thaliana*. Proc. Natl. Acad. Sci. USA **104:** 18830–18835.